WAVE-PARTICLE INTERACTIONS IN THE EVENING MAGNETOSPHERE DURING GEOMAGNETICALLY DISTURBED PERIODS

by

Roger Russell Anderson

A thesis submitted in partial fulfillment of the
requirements for the degree of Doctor of Philosophy
in the Department of Physics and Astronomy
in the Graduate College of
The University of Iowa

December, 1976

Thesis supervisor: Professor Donald A. Gurnett

Graduate College
The University of Iowa
Iowa City, Iowa 52242

CERTIFICATE OF APPROVAL

PH. D. THESIS

This is to certify that the Ph. D. thesis of

Roger Russell Anderson

has been approved by the Examining Committee for the thesis requirement for the Doctor of Philosophy degree in the Department of Physics and Astronomy at the December, 1976, graduation.

Thesis committee: Donald A. Hunnett
Thesis supervisor

Member

Member

Member

Member

ACKNOWLEDGMENTS

I am deeply indebted to the experimenters on S^3-A who allowed me the use of the unpublished data from their experiments in this research. I thank Dr. D. A. Gurnett for the use of the data from the University of Iowa plasma wave experiment, Drs. R. A. Hoffman and D. J. Williams for the use of the electron data from the GSFC and NOAA particle experiments, Dr. L. J. Cahill, Jr. for the use of the search coil and fluxgate magnetometer data from the University of Minnesota magnetometer experiments and Dr. N. C. Maynard for the use of the data from the GSFC static electric field experiment. This thesis was possible only because of the excellent cooperation of the above experimenters in providing me with ready access to their data. I am especially grateful to Dr. D. A. Gurnett for his support and advice over the many years I have known and worked with him. I also wish to thank Mrs. Chris Gloeckler and Dr. Paul H. Smith of Goddard Space Flight Center, Dr. N. K. Bewtra of Computer Sciences Corporation, and Drs. L. R. Lyons and J. N. Barfield and Mrs. Linda Bath of NOAA for their help in the computer analysis and preparation of the electron data.

For their assistance in processing the electric field data and helping in the preparation of the figures I wish to thank Dora Walker, Richard West, Byron Lundberg, Merlin Walters, Alan Lang,

and Stuart Waldman. I would like to thank Drs. Kaichi Maeda and Chris Goertz and Mr. Dave Sentman for their advice and suggestions. For her efficient, rapid and accurate typing of the manuscript, I thank Sandy Van Engelenhoven. The encouragement of Sandy, Bob Shaw, Bill Kurth and my many other friends in the Department of Physics and Astronomy has helped me and is very much appreciated. For their excellent work in the drafting of the illustrations I thank Joyce Chrisinger, Jeana Wonderlich, and John Birkbeck. For their efforts in the design, construction and testing of the S^3-A University of Iowa electric field experiment I thank Bill Pfeiffer, Dan Odem, Roger D. Anderson and Jim Cessna.

I am forever grateful for the love, support and encouragement of my family, Grace, Raymond, Carol and Bärbel. To you I dedicate this thesis.

This research was supported by the National Aeronautics and Space Administration under Contract NAS5-11167 and Grant NGL-16-001-043 and the Office of Naval Research.

ABSTRACT

Correlated wave and particle measurements obtained on the equatorially orbiting S^3-A satellite show that chorus and other whistler-mode VLF emissions are associated with enhanced fluxes of anisotropic low energy electrons (E ~ 1-10 keV) injected into the magnetosphere from the plasma sheet during geomagnetically disturbed periods. Continuous strong bands of whistler-mode noise are present outside the plasmasphere only when anisotropic low energy electron fluxes of the order of 10^7-10^8 $(cm^2 \text{ sec ster keV})^{-1}$ are present. Correlative studies of the electron pitch angle distributions and the whistler-mode spectra show that the upper cutoff frequency of the whistler-mode spectra increases with increasing pitch angle anisotropy of the cyclotron resonant electrons in agreement with the predictions of Kennel and Petschek [1966]. Growth rate calculations using the observed electron pitch angle distributions and intensities show good agreement between the calculated and observed whistler-mode spectra. Strong electrostatic emissions with frequencies above the local electron gyrofrequency, f_g, are shown to be associated with very low energy electrons ($E \leq 1$ keV) and are observed in several bands from near f_g up to the upper hybrid resonance frequency. An example where the frequency of the electrostatic emissions changes periodically at the same rate as a PC3 event observed at the same time is presented. These

observations are consistent with the electrostatic emissions being produced as a result of an anomalous perpendicular velocity distribution for hot electrons and the frequency of the emissions being determined by the ratio of the cold to hot electron number density and the upper hybrid resonance frequency.

TABLE OF CONTENTS

TABLE OF CONTENTS (Cont'd.)

LIST OF TABLES

LIST OF FIGURES

I. INTRODUCTION

During geomagnetically quiet periods the S^3-A orbit is usually within the plasmasphere in the evening sector. The predominant plasma wave activity observed at this time is plasmspheric hiss. Frequently a very weak narrow band of noise near the electron gyrofrequency, f_g, is also observed. During geomagnetically disturbed periods the plasmasphere is usually sufficiently compressed such that S^3-A can exit the plasmasphere and enter the outer magnetosphere. In the outer magnetosphere in the evening sector S^3-A can be engulfed with a large flux of low energy particles being convected inward as a result of the geomagnetic disturbance. Two types of moderately intense VLF emissions are observed that are associated with the enhanced fluxes of low energy electrons that are convected inward, electrostatic emissions above f_g and electromagnetic whistler-mode emissions (primarily chorus). In this report we describe the simultaneous plasma wave and particle observations and discuss some possible generation mechanisms for these two types of plasma waves during geomagnetically disturbed periods.

Magnetospheric observations of whistler-mode emissions made by the first high altitude satellite VLF experiment on OGO 1 indicated that the source of the emissions lies close to the equatorial plane [Dunckel and Helliwell, 1969]. Tsurutani and Smith [1974], in a study of ELF whistler-mode emissions observed on OGO 5, found that in

the midnight sector chorus was confined to regions very close to the magnetic equator indicating local generation. Both studies noted that the whistler-mode emissions occurred in regions of the magnetosphere where large fluxes of low energy electrons were likely to be observed. These investigations were, however, limited only to wave data. In this study, simultaneous data from both the plasma wave experiment and the particle detector experiments on the equatorial orbiting S^3-A satellite are used to examine wave-particle interactions in the magnetosphere near the magnetic equatorial plane. The orbit of S^3-A (initial apogee is 5.24 R_E, perigee is 222 km, inclination is 3.6° and orbital period is 7 hr. 49 min.) plus an extensive set of field and particle experiments make the satellite particularly favorable for studies of wave-particle interactions in the magnetosphere [Longanecker and Hoffman, 1973]. The plasma wave experiment instrumentation consists of a 16-channel spectrum analyzer which covers the frequency range from 35 Hz to 100 kHz [Anderson and Gurnett, 1973]. Both units are connected to a 5.08 meter tip-to-tip electric dipole antenna. The electron detection instrumentation used in this analysis consists of a cylindrical electrostatic analyzer-channel electron multiplier system measuring mean energies from 1.2 keV to 26 keV in eight energy intervals [Longanecker and Hoffman, 1973] and a solid state detector with four levels having mean energies from 55 keV to 400 keV [Williams et al., 1974]. Supplementary data from the flux gate and search coil magnetometer experiments and the static electric field experiment are also used.

Plasma waves in the magnetosphere, their characteristics and occurrence as a function of location and geomagnetic activity and their interactions with energetic particles have been extensively studied by past experiments. First we shall briefly review past investigations of chorus and electrostatic ($f > f_g$) emissions, the two types of emissions with which this study is most concerned. Chorus is an electromagnetic emission with $f < f_g$ that consists of many randomly occurring discrete tones lasting a few tenths of a second that either rise or fall in frequency. In a morphological survey of VLF emissions observed with the low altitude Injun 3 satellite, Taylor and Gurnett [1968] found that for VLF emissions (primarily ELF hiss, chorus and VLF hiss) the region of most intense emissions moved to lower latitudes (which correspond to lower L-shells at the equator) during geomagnetically disturbed times. The Injun 3 VLF experiment used a magnetic loop antenna as a sensor. Similar results were obtained by Barrington et al. [1971] using Alouette 2 data. The Alouette 2 data were obtained using an electric dipole antennas as a sensor. Taylor and Gurnett [1968] also found that often chorus was confined to lower latitudes than ELF hiss. Russell et al. [1969] conducted a morphological study of ELF noise using data from the search coil magnetometer experiment on OGO 3. They concluded that the source of burst-like noise was near the equator. Burtis and Helliwell [1969] reported observations of banded chorus in data from experiments using magnetic loop antennas on OGO 1 and OGO 3. Banded chorus is chorus that occurs in well defined frequency bands. The banded chorus was usually

observed at L shells of 4 or greater which suggested that the noise was observed primarily outside the plasmasphere. Occurrence of the banded chorus was positively correlated with magnetic activity. In a companion study of magnetospheric whistler-mode emissions with the OGO 1 satellite, Dunckel and Helliwell [1969] found that the upper-frequency limit of most of the observed emissions was proportional to the minimum electron gyrofrequency along the magnetic field line passing through the satellite. This was interpreted to mean that the source of the emissions lies close to the equatorial plane. Using OGO 5 search coil magnetometer data, Tsurutani and Smith [1974] studied ELF electromagnetic emissions in the midnight sector of the outer magnetosphere. They detected chorus in conjunction with magnetospheric substorms throughout the region from L = 5 to L = 9 but only during postmidnight hours. This chorus occurred most frequently at the geomagnetic equator and did not extend beyond $\pm$ 15° geomagnetic latitude. From this they concluded chorus was locally generated. They found the distribution of chorus as a function of L and local time to be strikingly similar to the distribution of enhanced, trapped and precipitated substorm electrons with energies $>$ 40 keV. The postmidnight occurrence of the chorus was attributed to the eastward curvature and gradient drift of the injected electrons.

The first direct associations between whistler-mode waves and energetic particles were made at low altitudes. Oliven and Gurnett [1968] observed that microbursts of E $\geq$ 40 keV electrons detected by the Injun 3 satellite were always accompanied by VLF chorus emissions.

Using high altitude balloons launched from Siple station, Antarctica (L = 4.2) Rosenberg et al. [1971] observed one-to-one correlations between short bursts of E > 30 keV x-rays and bursts of VLF emissions at 2.5 kHz. The energy of the electrons contributing to the x-ray bursts was estimated to be 30 to 100 keV. Burton and Holzer [1974], in a study of chorus in the outer magnetosphere, reported experimental support for the necessity of a critical pitch angle anisotropy for whistler-mode wave generation as proposed by Kennel and Petschek [1966]. On an OGO 5 pass through the nightside outer magnetosphere, Burton and Holzer [1974] observed that the region of maximum pitch angle anisotropy for 50 to 100 keV electrons coincided with the region of origin of chorus as identified by their wave normal analysis. Fredricks [1975] reviews some of the recent theoretical and experimental research regarding the association of chorus emissions and wave-particle interactions in the outer magnetosphere.

Intense magnetospheric electric field emissions near $3f_g/2$ were first observed by Kennel et al. [1970] on the OGO 5 satellite. These emissions were localized near the equator and were observed from 2100 to 1200 LT for $4 < L < 10$. Because of their high frequency and high electric field amplitudes (typically 1-10 mV m^{-1}), Kennel et al. [1970] suggested these emissions could be the source of strong pitch angle diffusion and energization of 1-10 keV auroral zone electrons. Scarf et al. [1973] showed that enhanced levels for $f \geq 3f_g/2$ electric field emissions were asscciated with substorm expansions. They found post-expansion $f \simeq 3f_g/2$ waves to be intense enough to

provide strong diffusion for $E > 50$-80 keV electrons and changes in the local pitch angle distributions were correlated with variations in wave amplitude levels. Electromagnetic chorus emissions were also observed during the substorm expansion phase, but they occurred later and with lower wave intensities than the $f \simeq 3f_g/2$ waves. Fredricks and Scarf [1973] using a more expanded set of OGO 5 data than Kennel et al. [1970] found that in the local time region from 1900 to 0700 LT the occurrence of emissions tended to be concentrated in the $5 \leq L \leq 7$ region. The emissions were also found to occur from $+40°$ to $-50°$ geomagnetic latitude. However the most intense $3f_g/2$ emissions were found near the geomagnetic equator and near local midnight which is the area at the base of the plasma sheet. Shaw and Gurnett [1975] have also observed $(n + 1/2)f_g$ electrostatic waves in the outer magnetosphere in data acquired using the long electric dipole antennas on IMP 6. Shaw and Gurnett [1975] suggested that the electrostatic noise bands they observed near the plasmapause were related to the upper hybrid resonance noise observed inside the plasmasphere and the $(n + 1/2)f_g$ waves observed in the outer magnetosphere.

II. SPACECRAFT AND EXPERIMENT DESCRIPTION

S^3-A (the Small Scientific Satellite -- Explorer 45) was launched from the San Marco Equatorial Range, Kenya, Africa, on November 15, 1971, into an eccentric equatorial orbit. The perigee altitude was 222 km, the apogee altitude was 27,031 km (5.24 R_E geocentric), the inclination was 3.57° and the orbital period was 7 hours 49 minutes. The initial apogee direction was 21.8 hrs. MLT (Magnetic Local Time) and this direction decreased at the rate of 0.8 hrs. per month. S^3-A was spin-stabilized with the spin axis near the ecliptic plane. The initial spin period was 16 seconds, but this was reduced a few weeks after launch to ~ 8.4 seconds for dynamic stability. The electric dipole antenna for the electric field experiments on S^3-A consisted of two graphite-coated spheres, 14 cm in diameter, mounted on booms such that the center-to-center distance between the spheres was 5.08 meters. Each sphere was connected to a high input impedance ($C_{in} \simeq 10$ pf, $R_{in} \simeq 50$ megohms) unity gain pre-amplifier mounted on the boom about halfway between the center of the sphere and the center of the spacecraft. The axis of the electric dipole antenna was perpendicular to the spacecraft spin axis.

The electronics instrumentation for the University of Iowa plasma wave experiment consists of two principal elements: (1) a step frequency spectrum analyzer, and (2) a wideband receiver

[Anderson and Gurnett, 1973]. The step frequency spectrum analyzer has 15 narrowband channels with center frequencies logarithmically spaced from 35 Hz to 100 kHz and one wideband channel with a bandpass of about 100 Hz to 10 kHz. The four highest frequency narrowband filters of the step frequency spectrum analyzer have bandwidths of $\pm$ 7.5% of their center frequencies, and the remaining narrowband filters have bandwidths of $\pm$ 15.0% of their center frequencies. A differential amplifier is used to provide a signal proportional to the potential difference between the antenna elements. The differential amplifier output signal drives all of the filters simultaneously. The filter outputs are then sequentially switched into an 80-db logarithmic detector to provide frequency spectrum measurements. The logarithmic detector output is a dc voltage proportional to the logarithm of the average input amplitude. The input amplitude range for a sine wave signal was from 10 μV to 100 mV (RMS). The time constant for the logarithmic detector was 0.04 seconds. The reprogrammable onboard data system controls the switching of the spectrum analyzer filters and the sampling of the logarithmic detector output. (This reprogrammable onboard data system performed satisfactorily until April, 1973.)

The wideband receiver is an 80 db automatic gain control (AGC) receiver with a bandwidth of about 100 Hz to 10 kHz. The minimum detectable sine wave signal for the AGC receiver is 10 μV RMS. The feedback time constant for the AGC network is $\sim$ 0.5 seconds. The output of the wideband receiver modulates the special purpose telemetry

transmitter. The wideband data are recorded on the ground and then are processed by a spectrum analyzer to produce high-resolution frequency-time spectrograms. The wideband system was normally operated one orbit out of three, but for special periods was operated continuously. The S^3-A wideband operations continued until the spacecraft was turned off in May, 1974.

The electron energy spectra and pitch angle distributions used in this study were obtained from the electron channeltron detector and solid-state electron detector which were mounted such that their look angles were perpendicular to the spacecraft spin axis. The channeltron detector consisted of a cylindrical electrostatic analyzer for particle species and energy selection and a channel electron multiplier as the sensor. The solid-state electron detector was a magnetic spectrometer with four surface barrier detectors. The energy windows established electronically were matched to the energy intervals from the magnetic dispersion of the beam by the magnet [Longanecker and Hoffman, 1973; Williams et al., 1974]. Table 1 shows the level designation, the mean energy and the energy range for the channeltron and solid-state electron detectors used in this analysis.

The static magnetic field measurements were made by a three-axis fluxgate magnetometer that had two ranges controlled by ground command: $\pm$ 3000γ with 6γ resolution and $\pm$ 300γ with 0.6γ resolution. The wideband analog magnetic field data were obtained using a permeable core search coil magnetometer with a frequency response from

1 Hz to 3 kHz [Parady and Cahill, 1973]. The 30 Hz to 3 kHz signals from the search coil magnetometer, amplified at a gain selectable by ground command, also modulated the special purpose transmitter and were transmitted to the ground simultaneously with the electric field wideband data.

III. CHARACTERISTICS OF THE PLASMA WAVES INVESTIGATED

A. Whistler-Mode Waves

The most common plasma wave phenomenon below the local electron gyrofrequency, f_g, observed outside the plasmasphere in the evening sector by S^3-A is chorus. Chorus is an electromagnetic whistler-mode emission that consists of short bursts of rising or falling tones. The bursts typically occur as frequently as ten times per second or even more often. The bursts can extend in frequency from 0.10 f_g up to about 0.75 f_g but usually lie in the range 0.25 f_g to 0.60 f_g. Several examples of chorus are shown in Figure 1. The top panel of each set is the frequency-time spectrogram of the wideband analog data from the search coil magnetometer experiment. The lower panel of each set contains the frequency-time spectrogram of the electric field wide-band analog data. The calibration marks for these spectrograms occur at one minute intervals and are 1 kHz apart in frequency. For reference, $f_g/2$ and f_g are indicated at the right side of each spectrogram. As indicated in the examples shown in Figure 1, chorus usually has a band of missing emissions near $f_g/2$. This is clearly illustrated in Figure 2, a one hour frequency-time spectrogram of electric field wide-band analog data for Orbit 115 on December 22, 1971. The integral half harmonics of the electron gyrofrequency are plotted on the spectrogram as fenced lines. Clearly the band of missing emissions

is centered near $f_g/2$. The width of the band of missing emissions can vary from as small as 100 Hz up to nearly 1 kHz; i.e. 2% to 20% of the typical 5 kHz electron gyrofrequency near apogee. Chorus is observed on almost every orbit that exits the plasmasphere during geomagnetically disturbed times in the evening sector. This is in sharp contrast to the observations of Tsurutani and Smith [1974] who observed no chorus prior to midnight. Later we will show that the occurrence of chorus is associated with the injection of low energy (1-10 keV) electrons into the evening sector during geomagnetic storms and substorms. On S^3-A chorus is observed only outside the plasmasphere. Sometimes it is sporadic -- a few weak bursts every few minutes -- but frequently it is nearly continuous.

B. Electrostatic $f > f_g$ Emissions

During geomagnetically disturbed times the most common emissions above f_g observed outside the plasmasphere in the evening sector are electrostatic emissions between harmonics of the electron gyrofrequency. We shall refer to these plasma waves as electrostatic $f > f_g$ emissions. In the literature they have also been called $\sim (n + 1/2)f_g$ electrostatic waves. As shown in the 0-10 kHz one-minute frequency-time spectrograms in Figure 3, the $f > f_g$ electrostatic emissions appear as several spin-modulated bands which can nearly cover the frequency range from f_g to 2 f_g. The arrows at the top of the spectrograms indicate when the electric dipole antenna is most nearly parallel to the ambient magnetic field. Since the nulls in the electric

field data are nearly coincident with when the electric dipole antenna is most nearly parallel to the ambient magnetic field, the electric field direction is thus determined to be nearly perpendicular to the ambient magnetic field. For electrostatic waves this indicates the propagation vector is also almost perpendicular to the ambient magnetic field. The fact that the emissions above f_g are electrostatic is indicated in Figure 4 which contains one-hour frequency-time spectrograms of both the search coil magnetometer data and the electric field data for Orbit 101. This one hour interval occurred during a geomagnetic storm of such intensity that near 1950 UT f_g fell to about 2.2 kHz and the emissions above f_g were below the ~ 3 kHz upper cutoff frequency for the search coil magnetometers. However, emissions above f_g were observed only in the electric field data. No emissions above f_g were observed either in the search coil magnetometer wideband analog or digital filter data [Parady and Cahill, 1973].

Figure 5 shows the electric field wideband analog data for the entire period beyond the plasmasphere for the Orbit 214. The banded structure of the electrostatic $f > f_g$ waves persists throughout the orbit although the ratio of the frequency of the most intense bands to the electron gyrofrequency changes. Near apogee the strongest bands were between 1.5 and 2.0 f_g while at lower altitudes the strongest bands were between 1.0 and 1.5 f_g. This is not a hard and fast rule, however. For example, the strongest electrostatic $f > f_g$ emissions for Orbit 115 shown in Figure 2 are between 1.0 and 1.5 f_g near apogee but are near or above 1.5 f_g as the altitude decreases.

As will be discussed in detail later, the frequency range of electrostatic $f > f_g$ emissions is strongly dependent on the ratio of cold to hot electrons and the ambient electron number density. Figure 6 contains the digital spectrum analyzer data for Orbit 214. Near apogee moderately intense electrostatic $f > f_g$ emissions are observed up to 31.1 kHz. For the measured gyrofrequency of 4.6 kHz, 31.1 kHz lies between 6 f_g and 7 f_g.

Like chorus, electrostatic $f > f_g$ emissions are observed on almost every orbit that exits the plasmasphere during geomagnetically disturbed periods. Inside the plasmasphere only the electrostatic emissions near the upper hybrid resonance (UHR) frequency are observed. Later we will show that electrostatic $f > f_g$ emissions observed outside the plasmapause are associated with very low energy electrons (energies typically 1 keV or lower) that are injected into the magnetosphere during geomagnetic storms and substorms.

IV. RELATIONSHIP OF WHISTLER-MODE WAVES TO THE ELECTRON DISTRIBUTION FUNCTION

A. Occurrence of Chorus as a Function of Low Energy Electron Intensity

Strong and nearly continuous bands of chorus are observed by S^3-A only when the satellite is outside the plasmasphere and then only when large fluxes of low energy electrons at energies appropriate for electron cyclotron resonance with the chorus waves are present. This correspondence is illustrated in Figures 7 and 8 for Orbit 35, which occurred on November 26, 1971. The top portion of Figure 7 contains plots of the differential directional electron intensity for $\alpha \sim 90°$ for electrons with mean energies from 1.2 keV to 100.0 keV for the entire orbit. The bottom portion of Figure 7 displays the electric field digital spectrum analyzer data from 1.0 kHz to 100.0 kHz for the same time period. To aid in identifying the plasma wave phenomena, the measured electron gyrofrequency, f_g, has been drawn in as a dashed line.

The two points marked PP at 0834 UT (L = 4.25 and MLT = 20.1 hrs.) and 1244 UT (L = 4.15 and MLT = 0.2 hrs.) are the outbound and inbound plasmapause crossings as determined by the static electric field experiment going into and coming out of saturation. The number density at the point of saturation for the static electric field experiment is 60 cm^{-3} to within a factor of 2 [Morgan and Maynard, 1976].

At the outbound plasmapause crossing the UHR noise identified by Gurnett and Shaw [1973] is observed to fall abruptly from 100.0 kHz to 31.1 kHz. $f_{UHR} = (f_p^2 + f_g^2)^{1/2}$ where f_p is the electron plasma frequency. Since f_p is several times larger than f_g, $f_{UHR} \sim f_p$. $f_p = 8.985 \sqrt{N}$ kHz where N is the electron number density measured in electrons cm^{-3}. Thus at the outbound plasmapause the UHR noise band indicates that N falls abruptly from ~ 124 cm^{-3} to ~ 12 cm^{-3} in excellent agreement with the determinations made by the static electric field experiment.

As indicated by the shaded area in Figure 7, just before 1100 UT (L = 5.15, MLT = 22.4 hrs.) and more than two hours after the outbound plasmapause crossing, the electron fluxes from 1.2 keV to 9.2 keV began to increase abruptly as the satellite encountered low energy particles being injected into the magnetosphere from the plasma sheet as a result of a substorm. Somewhat later abrupt enhancements occurred for electrons up to 25.6 keV and a slight enhancement was present even up to 55.0 keV. The peak intensities observed for the 1.2 keV and 1.8 keV electrons were about 10^8 electrons $(cm^2 \text{ sec ster keV})^{-1}$. The intensities decreased with increasing energy such that the peak intensities for the 9.2 keV and 13.5 keV electrons were about 10^7 electrons $(cm^2 \text{ sec ster keV})^{-1}$. The peak intensities for all electrons from 1.2 keV to 25.6 keV were about an order of magnitude greater than the intensities just prior to the enhancements.

Shortly after the abrupt enhancements begin and at about the time the maximum intensity is observed for electrons from 1.2 keV to

9.2 keV, strong and nearly continuous bands of chorus are evident. Because the chorus is impulsive, the peak values are typically much higher than the average values. The peak amplitudes of the chorus range from about 2 mV m^{-1} for the 1.78 kHz and 3.11 kHz channels at ~ 1120 UT to about 10 mV m^{-1} for the 5.62 kHz channel at ~ 1220 UT. Frequency-time spectrograms of the search coil magnetometer and electric field wideband analog data for the time period covering the electron enhancement are shown in Figure 8. These spectrograms show that the most intense chorus bands lie between ~ 0.4 f_g and ~ 0.6 f_g. The energy of electrons in cyclotron resonance with whistler-mode waves of frequency f is $E_R = E_B \frac{f_g}{f} (1 - \frac{f}{f_g})^3$ where $E_B = B^2/8\pi N$, the magnetic energy per particle. B is the magnitude of the static magnetic field. Expressed in terms of the electron gyrofrequency and the electron plasma frequency, $E_B = 255.4 \text{ keV} \times f_g^2/f_p^2$. The UHR noise evident in the bottom panel of Figure 7 for the period of the electron enhancement indicates f_p ~ 31.1 kHz. For this same time period f_g increases from ~ 5.0 kHz to ~ 11.5 kHz. Near the beginning of the electron enhancement, E_R's for 0.4 f_g and 0.6 f_g waves are 3.6 keV and 0.7 keV. Beginning about 1125 UT intense chorus is observed down to ~ 1.4 kHz which is ~ 0.25 f_g since f_g ~ 5.6 kHz. E_R for this frequency is 11.1 keV. At ~ 1220 UT, f_g = ~ 9.5 kHz. E_R's for 0.25 f_g, 0.4 f_g and 0.6 f_g are 40.2 keV, 12.9 keV and 2.5 keV. Thus throughout the time of the electron enhancement, the energies of the enhanced electrons are the energies appropriate for cyclotron resonance with the observed waves.

For Orbit 35 the low energy electron intensities remained high until just prior to the inbound plasmapause crossing then they abruptly dropped more than an order of magnitude. At this time the intense bands of chorus ceased.

As indicated in Figure 7, sporadic but moderately intense bursts of chorus were present throughout the outer magnetosphere from the outbound plasmapause crossing until the abrupt electron enhancement. These bursts were due to the relatively high background level of low energy electrons due to prior geomagnetic disturbances. Figure 9 is a plot of equatorial D_{st} from November 17 to November 30, 1971 [Sugiura and Poros, 1973]. Orbit 35 occurred about a day after geomagnetic disturbances which had been active for nearly a week reached peak intensity and slowly began to subside. In Figure 10 we have plotted the differential directional intensity of electrons for two periods: outbound $L = 5.0$ for Orbit 35 prior to the electron enhancement, inbound $L = 5.0$ during the electron enhancement. For comparison we have also plotted the average directional differential intensity at $L = 5.2$ reported by Lyons and Williams [1975] for a one week quiet period in December 1971. Due to the high level of geomagnetic disturbances, the ambient level for the low energy electrons is considerably higher than the quiet time levels even before the abrupt electron enhancement.

A second example of the close association between strong and nearly continuous bands of chorus and high intensities of low energy electrons is shown in Figure 11 for Orbit 36 on November 26, 1971. An abrupt increase in the intensities of low energy electrons from

1.2 keV to 9.2 keV began about 1840 UT more than one hour after the outbound plasmapause crossing. From ~ 1840 UT on enhanced fluxes of low energy electrons up to 13.5 keV were observed until just before the inbound plasmapause crossing. The peak electron intensities observed ranged from 7×10^7 electrons $(cm^2 \text{ sec ster keV})^{-1}$ at 1.2 keV and 6×10^7 electrons $(cm^2 \text{ sec ster keV})^{-1}$ from 1.8 to 4.0 keV to 10^7 electrons $(cm^2 \text{ sec ster keV})^{-1}$ at 9.2 keV and 3×10^6 electrons $(cm^2 \text{ sec ster keV})^{-1}$ at 13.5 keV. In the electric field data strong continuous bands of chorus were observed from ~ 1848 UT until just before the inbound plasmapause crossing. The most intense chorus with peak amplitudes up to 10 mV m^{-1} in the 3.11 kHz channel and 2 mV m^{-1} in the 1.78 kHz channel occurred around 1900 UT at the same time as the peak intensity was observed for all electrons from 1.2 keV to 13.5 keV. As the satellite moved inward, the low energy electron intensities gradually decreased until just before the plasmapause crossing where they dropped abruptly. Similarly the chorus amplitudes tended to decrease as the satellite moved inward.

A third example of the relationship between enhanced low energy electrons and the occurrence of chorus is shown in Figure 12 for Orbit 115 on December 22, 1971. For this orbit both the low energy electron enhancement and the moderately intense chorus bands begin and end nearly coincident with outbound and inbound plasmapause crossings. Just prior to the outbound plasmapause crossing at 0806 UT (L = 5.15, MLT = 21.5 hrs.) the differential directional intensities of all the low energy electron channels were less than 2×10^6 electrons $(cm^2 \text{ sec ster keV})^{-1}$. The peak intensities observed

following the outbound plasmapause crossing ranged from 9×10^7 electrons $(cm^2 \text{ sec ster keV})^{-1}$ at 1.8 keV to 1.2×10^7 electrons $(cm^2 \text{ sec ster keV})^{-1}$ at 6.0 keV. No enhancement in electron intensities above 6.0 keV was observed. Just prior to the inbound plasmapause crossing at 0944 UT (L = 4.09, MLT = 23.2 hrs.) all the low energy electron intensities fell abruptly to levels below 4×10^6 $(cm^2 \text{ sec ster keV})^{-1}$.

VLF chorus emissions began coincident with the abrupt increase in low energy electron intensities and terminated when the low energy electron intensities began to drop. This is clearly illustrated in Figure 13 where both the differential directional electron intensities and the electric field wideband analog data from ~ 0730 UT to 1000 UT are presented. The peak chorus amplitude observed during the period outside the plasmasphere was 700 $\mu V\ m^{-1}$.

The situation where the low energy electron enhancement begins just outside the outbound plasmapause crossing exists when the electron trough normally observed between the plasmasphere and the plasma sheet in the premidnight evening sector becomes filled in with low energy electrons during geomagnetically disturbed periods. This is shown schematically in Figure 14. Panel (a) shows the normal quiet time condition of the evening magnetosphere along with the S^3-A orbit trajectory appropriate for November and December, 1971. During quiet times the orbit of S^3-A seldom exits the plasmasphere in the evening sector. Panels (b) and (c) show the state of the evening magnetosphere for Orbit 35 and Orbit 36. During periods of increased geomagnetic

disturbances the plasmasphere is compressed to the extent that S^3-A can exit the plasmasphere and enter the region where the electron trough exists. As the satellite approaches local midnight it encounters high fluxes of low energy particles being convected into the magnetosphere from the plasma sheet as a result of the geomagnetic disturbances. These high fluxes of low energy electrons are observed until the satellite re-enters the plasmasphere. Panel (d) shows the situation for Orbit 115. The low energy electrons convected in from the plasma sheet have filled the electron trough in the region through which the satellite passes. Thus as soon as the satellite exits the plasmasphere it encounters the enhanced fluxes of low energy electrons. In order for the trough to be filled in with low energy electrons, the injection region must extend to earlier local times than that at the position of the satellite since the electrons drift eastward toward local midnight and then to dawn.

B. Chorus Spectra as a Function of Resonant Electron Anisotropy

The spectra of whistler-mode waves that interact with electrons via the cyclotron resonant interaction are dependent on the anisotropy of the resonant particles. The growth rate derived by Kennel and Petschek [1966] and which will be examined in detail in Section VI includes a term proportional to $A - \frac{1}{f_g/f-1}$ where A is the anisotropy and is defined as

$$A = \left. \frac{\int_o^\infty V_\perp \, dV_\perp \tan\alpha \frac{\partial F}{\partial \alpha}}{2\int_o^\infty V_\perp \, dV_\perp F} \right|_{V_\parallel = V_R}$$

where $V_\perp$ and $V_{||}$ are electron velocities perpendicular and parallel to the static magnetic field, F is the electron distribution function and V_R is the velocity of electrons in resonance with the waves. For a distribution function whose angular dependence varies as $\sin^m \alpha$, the anisotropy factor A is equal to $\frac{m}{2}$. A given set of electrons will contribute to whistler-mode wave growth if A for that set of electrons evaluated at $V_{||} = V_R$ is greater than $\frac{1}{f_g/f-1}$. For a given anisotropy wave growth will be supported only up to a cutoff frequency, f_c, determined by $A = \frac{1}{f_g/f_c-1}$. The factor $A - \frac{1}{f_g/f-1}$ is negative for $f > f_c$ and no wave growth will occur. For a $\sin^m \alpha$ distribution, $f_c/f_g = m/(m + 2)$. Thus for a distribution proportional to $\sin^2 \alpha$, $A = 1$ and $f_c = 0.5\ f_g$ and for a distribution proportional to $\sin^2 \alpha$, $A = 1.5$ and $f_c = 0.6\ f_g$.

An example of the relationship between the spectra of the chorus and the anisotropy of the resonant electrons is illustrated in Figure 15. At the top of the figure are the wideband analog frequency time spectrograms for the magnetic field and electric field data for 1833 UT to 1927 UT for Orbit 36. The bottom portion of the figure contains plots of the pitch angle distributions at five minute intervals for the electrons from 1.2 keV up to 25.6 keV. For each small square the scale on the axis of abscissas is 0° to 180° pitch angle and the scale on the axis or ordinates is $\log_{10}$ electrons $(cm^2$ sec ster keV$)^{-1}$ and full scale covers five orders of magnitude of electron intensity. Since the pitch angle plots are generated from left to right according to increasing L-value, time increases from right to left for the inbound portion of the orbit. The slanted lines

between the bottom of the electric field spectrogram and the top of the pitch angle plots show when the pitch angle plots were made.

As shown in the wideband analog spectrograms an intense chorus band with frequencies from 0.52 f_g to 0.70 f_g was present from 1848 UT to 1903 UT. f_g was 4.77 kHz at 1848 UT and increased to 5.00 kHz at 1903 UT. The peak amplitudes of the chorus band ranged from 700 $\mu V\ m^{-1}$ to 8 $mV\ m^{-1}$ and were typically a few $mV\ m^{-1}$. Only a very weak band near $f = 0.44\ f_g$ is evident below 0.5 f_g. As can be seen by comparing the pitch angle distributions at the bottom of Figure 15 with the wideband analog data, the intense chorus band with frequencies almost entirely greater than 0.5 f_g occurs simultaneously with extremely anisotropic pitch angle distributions for the cyclotron resonant electrons, especially at 4.0 and 6.0 keV. At ~ 1856 UT the pitch angle distributions for the 4.0 and 6.0 keV electrons are proportional to $0.85 \sin^7 \alpha + 0.15 \sin^{0.1} \alpha$ and $0.80 \sin^{10} \alpha + 0.20 \sin^{0.2} \alpha$, respectively. At ~ 1900 UT the pitch angle distributions for the 4.0 and 6.0 keV electrons are $0.80 \sin^{12} \alpha + 0.20 \sin^{0.2} \alpha$ and $0.70 \sin^{12} \alpha + 0.30 \sin^{0.2} \alpha$, respectively. As shown in Figure 16, between 1902:40 UT and 1904:30 UT, the 4.0 and 6.0 keV pitch angle distributions changed abruptly to less anistropic distributions with the dominant term proportional to only $\sin^3 \alpha$. At the same time the frequency limits of the chorus bands dropped to the range 0.30 f_g to 0.60 f_g with the maximum amplitudes below 0.5 f_g. According to the predictions of Kennel and Petschek [1966], a $\sin^3 \alpha$ distribution can

support wave growth only up to 0.6 f_g. Wave growth up to 0.70 f_g requires at least a $\sin^{4.67}\alpha$ distribution.

The digital spectrum analyzer data in Figure 11 indicate that between 1848 and 1903 UT the UHR frequency was between 16.5 and 31.1 kHz. Since $f_g \sim 5$ kHz, this requires the ambient number density to lie between 3 cm^{-3} and 12 cm^{-3}. For f_g = 5.0 kHz and N = 8 cm^{-3}, f_p = 25.4 kHz, f_{UHR} = 25.9 kHz and $E_B = B^2/8\pi N$ = 255.4 keV x f_g^2/f_p^2 = 9.9 keV. The parallel resonant energy, E_R, for f = 0.5 f_g, 0.6 f_g and 0.7 f_g waves would be 2.5 keV, 1.1 keV and 0.4 keV, respectively. The corresponding energies for N = 3 cm^{-3} would be 6.7 keV, 2.9 keV and 1.1 keV and the corresponding energies for N = 12 cm^{-3} would be 1.7 keV, 0.7 keV and 0.3 keV. Later we will show that the best agreement between the observed wave spectrum and the calculated growth rates occurs for $N \sim 8$ cm^{-3}, the number density we will assume for the following calculations.

For pitch angles, α, other than zero, the resonant energy is $E_{R\alpha} = E_R/\cos^2\alpha$. For f = 0.5 f_g, the resonant pitch angles for 4.0 and 6.0 keV electrons are 38° and 50°, respectively. For f = 0.6 f_g, the resonant pitch angles are 58° and 65°. For f = 0.7 f_g, the resonant pitch angles are 72° and 75°. In Figures 15 and 16 we see that the slopes of the 4.0 and 6.0 keV pitch angle distributions are the largest for α from about 45° to about 75°. The slopes of the pitch angle distributions in this range are sufficiently large to account for the observed instability. The pitch angle distributions are less steep near the resonant pitch angles for 0.5 f_g waves but

wave growth is still possible because waves near 0.5 f_g require only an anisotropy as great as that provided by a $\sin^2 \alpha$ distribution.

Wave growth also depends on the number of resonant particles. For the very anisotropic distributions described for the 4.0 and 6.0 keV electrons from 1848 to 1903 UT, wave growth at higher frequencies is predominant because the higher frequencies are resonant at larger pitch angles and the number of electrons increases significantly at larger pitch angles. For example, at 1856 UT, where the 4.0 keV electron pitch angle distribution was proportional to $0.85 \sin^7 \alpha + 0.15 \sin^{0.1} \alpha$, the fraction of electrons at 38°, 58° and 72° as compared to the number of electrons at 90°, are 0.171, 0.416 and 0.747, respectively. At 1900 UT where the 4.0 keV electron pitch angle distribution was proportional to $0.80 \sin^{12} \alpha + 0.20 \sin^{0.2} \alpha$, the fractions are 0.184, 0.304, and 0.636. At 1856 UT, where the 6.0 keV electron pitch distribution was proportional to $0.80 \sin^{10} \alpha + 0.20 \sin^{0.2} \alpha$, the ratios of electrons at 50°, 65° and 75° to the number of electrons at 90° are 0.245, 0.495 and 0.764. At 1900 UT where the 6.0 keV distribution was proportional to $0.70 \sin^{12} \alpha + 0.30 \sin^{0.2} \alpha$, the ratios are 0.313, 0.509 and 0.760.

The wave particle interactions occurring from 1848 UT to 1903 UT can be explained qualitatively as follows: The injection source provided a large number of 4-6 keV electrons with pitch angle distributions strongly peaked near 90°. These particles resonanted with whistler-mode waves and intense chorus bands were produced. The chorus was of such intensity to quickly diffuse the particles

toward smaller pitch angles and less anisotropic distributions. However, as long as the injection source provided fresh highly anisotropic electron fluxes, the equilibrium distribution was highly anisotropic. But once the injection of highly anisotropic electrons ceased, the strong pitch angle diffusion caused by the intense chorus quickly changed the pitch angle distribution to a less anisotropic one. Chorus waves will still resonate with the less anisotropic electron distributions but the wave growth is at lower frequencies and is less intense. Since the chorus intensities are less, only weak pitch-angle diffusion results and the pitch angle distributions change much more slowly.

C. Chorus Damping as a Function of Resonant Electron Pitch-Angle Distribution

In both the digital spectrum analyzer data and the wideband analog data in Figures 12 and 13 for Orbit 115 it is apparent that the chorus amplitude decreased significantly from ~ 0826 UT to ~ 0837 UT and from ~ 0856 UT to ~ 0908 UT. From the pitch angle distributions shown in Figure 17 we see that during the periods chorus was weak or absent, the pitch angle distributions from $\alpha \sim 60°$ to $\sim 120°$ for the cyclotron resonant electrons were nearly flat or even displayed a relative minimum near $\alpha = 90°$. The Kennel and Petschek [1966] theory predicts zero wave growth for flat distributions and wave damping for distributions which are concave at the cyclotron resonant energy. Around 0832 UT the 2.7 keV electron distribution was nearly flat from $\alpha \sim 55°$ to $\sim 125°$ and the 4.0 keV electron

distribution was concave from $\alpha \sim 55°$ to $\sim 125°$. Around 0900 UT the pitch angle distributions for energies at and below 4.0 keV are peaked near $\alpha = 90°$ while the 6.0 keV distribution is flat if not slightly concave from $\alpha \sim 60°$ to $\sim 120°$. At 0832 UT $f_g = 5.78$ kHz and at 0900 UT $f_g = 7.08$ kHz. The strong UHR band in the 31.1 kHz spectrum analyzer channel indicates that $f_p \sim 31$ kHz. Thus $E_B = 8.8$ keV at 0832 UT and 13.2 keV at 0900. For waves with $f = 0.6\ f_g$, a frequency near where the chorus spectra peaks for Orbit 115, $E_R =$ 0.94 keV at 0832 and 1.4 keV at 0900 UT. At 0832 UT the pitch angles where electrons with 2.7 keV and 4.0 keV energies would be in cyclotron resonance with 0.6 f_g waves would be $\sim 54°$ and $\sim 61°$. At 0900 UT 6.0 keV electrons would be in cyclotron resonance with $f =$ 0.6 f_g waves at $\alpha \sim 61°$. The observed flat or concave pitch angle distributions thus will cause zero wave growth or damping for waves at frequencies where previously the peak chorus intensity had been observed because the pitch angles appropriate for cyclotron resonance lie on the flat portion of the distribution.

D. Half-Gyrofrequency Whistler-Mode Waves and Their Relationship to Electron Anisotropies Inside the Plasmasphere

A moderately strong electric field emission associated with electrons and observed during geomagnetically disturbed periods inside the plasmasphere is prominant in Figure 11 for Orbit 36 from about 1515 UT to 1600 UT first in the 16.5 kHz channel and later in the 10.0 kHz channel. The peak amplitude of $\sim 200\ \mu V\ m^{-1}$ for the 16.5 kHz channel occurred at $\sim$ 1526 UT when $f_g = 28.4$ kHz. The peak amplitude of $\sim 60\ \mu V\ m^{-1}$ for the 10.0 kHz channel occurred at $\sim$ 1543 UT when

f_g = 18.5 kHz. Thus the peak amplitudes in the 16.5 kHz and 10.0 kHz channels occurred for waves at 0.58 f_g and 0.54 f_g, respectively, indicating that the observed noise band is centered slightly above 0.5 f_g. These waves exist at too high of a frequency to ascertain whether or not they have a magnetic component. However, on many orbits where chorus is present just outside the plasmapause, these $\sim f_g/2$ waves appear to be a continuation of the chorus bands except that they tend to have lower amplitudes than the chorus and they are less burst-like and rather tend to be more diffuse and continuous similar to hiss. Since these waves have characteristics similar to chorus and hiss, both whistler-mode waves, we shall assume they also are whistler-mode waves.

The intense UHR noise at 1539 UT in the 100 kHz channel indicates $f_p \sim 100$ kHz. At that time f_g = 19.9 kHz so that E_B = 10.1 keV. For waves with frequency f = 0.55 f_g, E_R = 1.7 keV. The pitch angle distributions for 1.2 keV to 25.6 keV electrons for 1535 UT to 1610 UT are shown in Figure 18. Near 1540 UT the differential directional intensity of 1.8 keV electrons at $\alpha = 90°$ was $\sim 1.0 \times 10^7$ electrons $(cm^2 \text{ sec ster keV})^{-1}$. The pitch angle distributions for all electrons from 1.2 keV to 25.6 keV could be characterized as at least $\sin^3 \alpha$ or $\sin^4 \alpha$ distributions. The upper cutoff frequency for such distributions is 0.60 f_g or 0.67 f_g. The anisotropies observed for the electrons which are resonant with the $f \sim f_g/2$ waves are sufficient to produce wave growth at the observed frequencies. Little evidence of half-gyrofrequency whistler-mode waves appear after 1600 UT. In

the pitch angle distribution plots we see that at this time the low energy electrons become much less anisotropic although the $\alpha = 90°$ intensity remains nearly the same. At 1610 UT the pitch angle distributions are less anisotropic than a sin α distribution and thus would not support wave growth above $0.33\ f_g$.

V. RELATIONSHIP OF ELECTROSTATIC $f > f_g$ WAVES TO THE ELECTRON DISTRIBUTION FUNCTION

A. Occurrence of Electrostatic $f > f_g$ Waves as a Function of Low Energy Electron Intensity and Pitch Angle Anisotropy

Electrostatic waves between harmonics of the electron gyrofrequency are observed in the evening sector on almost every pass that exits the plasmasphere during geomagnetically disturbed times. These electrostatic $f > f_g$ waves usually begin coincident with or slightly before the abrupt enhancement in low energy electrons is observed. These electrostatic waves are believed to be generated by anomalous perpendicular electron velocity distributions at very low energies most likely below the minimum observed energy on S^3-A. Electrostatic $f > f_g$ emissions were observed on each of three orbits we have already discussed in regard to chorus: Orbit 35 (Figures 7 and 8), Orbit 36 (Figures 11 and 15) and Orbit 115 (Figures 2, 12 and 13).

On Orbit 35 a relatively weak band of electrostatic emissions between 1.25 f_g and 1.50 f_g begins nearly coincident with abrupt enhancement of low energy electrons and remains until the enhancement ends at the inbound plasmapause crossing. Higher frequency electrostatic emissions are weakly evident in the digital spectrum analyzer data up to 3 f_g.

On Orbit 36 (Figures 11 and 15) a moderately strong electrostatic emission ranging from ~ 1.0 f_g to 1.5 f_g begins coincident

with the abrupt enhancement in low energy electrons and precedes the strong chorus bands by about ten minutes. For Orbit 36 the influx of low energy electrons from the plasma sheet was first observed in the 1.2 keV channel at ~ 1738 UT, in the 1.8 keV channel at ~ 1757 UT and in the 2.7 keV channel ~ 1831 UT. This observation is consistent with the plasma sheet being convected inward. The leading edge of the plasma sheet contains the lowest energy particles. Deeper inside the plasma sheet the energy density increases. The fact that the electrostatic $f > f_g$ emissions precede the chorus indicates that they are associated with lower energy electrons than those that resonate with the chorus.

For Orbit 115 (Figures, 2, 12 and 13) intense electrostatic emissions up to 6 f_g were observed associated with the low energy electron enhancement. Electrostatic emissions between 1.0 f_g and 1.5 f_g actually preceded the enhancement by five minutes. The electrostatic $f > f_g$ emissions began at 0805 UT while the 1.8 keV electron intensity abruptly increased at 0810 UT. The electron intensities at 2.7 keV and 4.0 keV abruptly increased at 0816 UT and 0820 UT. The electrostatic $f > f_g$ emissions observed on Orbit 115 were some of the most intense and most broadband emissions observed on S^3-A. The peak amplitudes observed were 1.2 mV m^{-1} for the 5.62 kHz channel, 3.6 mV m^{-1} for the 10 kHz channel and 1.7 mV m^{-1} for both the 16.5 kHz and 31.1 kHz channels.

Further evidence that the electrostatic $f > f_g$ emissions are associated with very low energy electrons is provided by the data for

Orbit 67 on December 6, 1971. In the electric field digital spectrum analyzer data at the bottom of Figure 19 we see that outside the plasmapause only electric field emissions above f_g are present: an intense band of UHR noise and a moderately strong electrostatic band near 1.5 f_g. No emissions below f_g are evident either in the wide-band analog data in Figure 20. In the differential directional electron plots in the top of Figure 19, only the very lowest energy electrons (E = 1.2 keV) display an enhanced intensity outside the plasmapause. In Figure 21 we have plotted the $\alpha \sim 90°$ electron energy spectra at L = 5.2 for Orbits 66, 67 and 68 and also the mean quiet time levels for Orbits 75-97 from Lyons and Williams [1975]. At and above 1.8 keV, the spectra for Orbits 66, 67 and 68 are near the mean quiet time levels. For Orbits 66 and 68 which do not exit the plasmasphere the 1.2 keV energy spectra are near the projected mean quiet time levels. But for Orbit 67 which does exit the plasmasphere, the 1.2 keV electron intensity, which reaches a peak of 8×10^7 electrons $(cm^2 \text{ sec ster keV})^{-1}$, is more than an order of magnitude greater than the 1.2 keV electron intensities for Orbits 66 and 68. As shown in Figure 22, only the pitch angle distributions for the 1.2 keV electrons are very anisotropic for the entire period the satellite is outside the plasmasphere. The $\alpha \sim 90°$ electron intensities are more than 8 times greater than the $\alpha \sim 30°$ electron intensities for the 1.2 keV electrons. For all energies above 1.2 keV, the pitch angle distributions are nearly isotropic.

B. Correspondence Between Quasi-Periodic Frequency Limit Changes for Electrostatic $f > f_g$ Emissions and PC3 Micropulsations

An unusual feature of electrostatic $f > f_g$ emissions shown in Figure 20 for Orbit 67 is that frequency of the emission bands changes quasi-periodically from being above 1.5 f_g to being below 1.5 f_g. From 1830 UT to 1845 UT this change is nearly periodic with a period of ~ 67 seconds. Around 1940 UT the period is about 85 seconds. Throughout the time of the occurrence of electrostatic emissions on Orbit 67, PC3 micropulsations were observed by the ground station at College, Alaska. From ~ 1850 to 1905 UT the micropulsations were quite periodic with a period of ~ 63 seconds [R. R. Heacock, private communication, 1976]. Although the periods are not identical, the presence of micropulsations on the ground indicates they should also be present at the satellite. The difference in both L and latitude between the satellite and the ground station could account for the difference in periods. The frequency of the electrostatic emissions according to the theories of their generation is dependent on the ratio of the number density of ambient cold electrons to the number density of warm electrons. The quasi-periodic change in the frequency of the electrostatic emissions observed on Orbit 67 can be explained by PC3 micropulsations at the satellite's location modulating either the ambient electron number density or the very low energy warm electron number density.

VI. A REVIEW OF ELECTRON CYCLOTRON RESONANCE INTERACTIONS AND COMPARISON BETWEEN PREDICTED WHISTLER-MODE GROWTH RATES AND OBSERVED SPECTRA

A. Whistler-Mode Wave Amplification as a Result of Low Energy Electron Cyclotron Resonant Interactions

Kennel and Petschek [1966] derived an expression for the growth rate of whistler-mode waves due to the electron cyclotron resonance interaction. They began their analysis with the Vlasov-Maxwell equations for a two-component collision-free plasma of ions and electrons,

$$\frac{\partial f_{\pm}^{+}}{\partial t} + \vec{V} \cdot \nabla f_{\pm}^{+} \pm \frac{e}{m_{\pm}} \left[\vec{E} + \frac{\vec{V}\times\vec{B}}{c}\right] \cdot \frac{\partial f_{\pm}^{+}}{\partial \vec{V}} = 0,$$

$$\nabla \cdot \vec{E} = 4\pi e \int d^3V (f^{+} - f^{-}),$$

$$\nabla \times \vec{E} = -\frac{1}{c}\frac{\partial \vec{B}}{\partial t},$$

$$\nabla \times \vec{B} = \frac{4\pi e}{c} \int d^3V \, \vec{V}(f^{+} - f^{-}) + \frac{1}{c}\frac{\partial \vec{E}}{\partial t} \quad \text{and}$$

$$\nabla \cdot \vec{B} = 0, \text{ where}$$

$f_{\pm}^{+}(\vec{X}, \vec{V}, t)$ was the one particle distribution function for each species with the positive superscript for the ions and negative superscript for the electrons. e is the electronic change and $m_{\pm}^{+}$ is

the mass of each species. They assumed there were no zero-order electric field, spatial gradients or time variations. For convenience, the equilibrium magnetic field was assumed to be only in the $\hat{Z}$ direction. They allowed the equilibrium state to be varied by small perturbations of the form

$$f^{\pm}(\vec{X}, \vec{V}, t) = MF^{\pm}(\vec{V}) + \delta f^{\pm}(\vec{V}) e^{i(kz-\omega t)},$$

$$\vec{B}(\vec{X}, t) = B_o \hat{Z} + \delta\vec{B} e^{i(kz-\omega t)}, \text{ and}$$

$$\vec{E}(\vec{X}, t) = 0 + \delta\vec{E} e^{i(kz-\omega t)}$$

and substituted these expressions into the Vlasov-Maxwell equations, disregarding nonlinear terms in the perturbation. For parallel propagating right-handed circularly polarized waves they obtained the dispersion relation

$$n^2 = R = 1 - \pi \sum_{+,-} \frac{(\omega_p^{\pm})^2}{\omega} \int_0^{\infty} V_\perp^2 \, dV_\perp \int_{-\infty}^{\infty} dV_{||}$$

$$\cdot \left[\frac{\partial F^{\pm}}{\partial V_\perp} - \frac{k}{\omega}\left(V_{||} \frac{\partial F^{\pm}}{\partial V_\perp} - V_\perp \frac{\partial F^{\pm}}{\partial V_{||}}\right)\right] \left[\frac{1}{kV_{||} - \omega - \Omega^{\pm}}\right] \qquad (1)$$

where

$$\omega_p^{\pm} = \sqrt{4\pi Ne^2/m^{\pm}} \quad \text{and} \quad \Omega^{\pm} = \frac{\pm eB}{m^{\pm}c} .$$

For $\Omega^+ \ll \omega < |\Omega^-|$, $n^2 = R$ is the whistler mode. By assuming the plasma to be cold, i.e., $F^{\pm} = \frac{1}{2\pi}\,\delta(V_\perp)\,\delta(V_{||})$, $n^2 = R$ reduces to

$$n^2 = 1 - \frac{(\omega_p{}^+)^2}{\omega(\omega+\Omega^+)} - \frac{(\omega_p{}^-)^2}{\omega(\omega+\Omega^-)} \,. \tag{2}$$

The limits on the wave frequency, $\Omega^+ \ll \omega < |\Omega^-|$, allows one to neglect the ion contribution since it is only a fraction, m^-/m^+, of the electron contribution. And if the plasma frequency is at least a few times larger than the gyrofrequency, then $n^2 \gg 1$ and for the $n^2 = R$ mode,

$$R_e(n^2) \approx \frac{(\omega_p{}^-)^2}{\omega(|\Omega^-|-\omega)} \equiv \frac{f_p{}^2}{f(f_g-f)} \,. \tag{3}$$

The cyclotron resonance phenomenon results from the resonant denominator in Equation 1, $(kV_{||}-\omega-\Omega^{\pm})$. When this denominator is zero, the velocity space integration pick up an imaginary part. For electron cyclotron resonsnce, the parallel resonant velocity is defined by

$$kV_R - \omega - \Omega^- = 0 \text{ or } V_R = \frac{-|\Omega^-|+\omega}{k} \,. \tag{4}$$

For electrons whose velocity parallel to the external magnetic field equals V_R but who are travelling in the opposite direction of the wave, the wave frequency will be doppler shifted to the electron gyrofrequency. Since violation of the first adiabatic invariant, a

change in pitch angle without a change in energy, can only occur if a particle is subject to field fluctuations near its own gyrofrequency, electrons with parallel velocity V_R can have their pitch angles easily changed without a corresponding significant change in energy.

For non-relativistic electrons, the cyclotron resonant energy, E_R, equals $\frac{1}{2}m_e V_R^2$.

$$E_R = \frac{1}{2}m_e V_R^2 = \frac{1}{2}m_e \frac{(\omega - |\Omega^-|)^2}{k^2} .$$

From Equation 3, we see

$$\frac{c^2k^2}{\omega^2} = n^2 \approx \frac{(\omega_p^-)^2}{\omega(|\Omega^-| - \omega)} .$$

Thus

$$E_R = \frac{1}{2}m_e \frac{(\omega - |\Omega^-|)^2 c^2}{\omega^2(\omega_p^-)^2} \omega(|\Omega^-| - \omega)$$

$$= \frac{1}{2}m_e \frac{(|\Omega^-| - \omega)^3 c^2}{\omega(\omega_p^-)^2} = \frac{\frac{1}{2}m_e |\Omega^-|^3 c^2 (1 - \frac{\omega}{|\Omega^-|})^3}{\omega(\omega_p^-)^2}$$

Using the definitions of ω_p^- and Ω^- this reduces to

$$E_R = \frac{1}{2}m_e c^2 \frac{e^2 B^2}{m_e^2 c^2} \frac{m_e}{4\pi Ne^2} \frac{|\Omega^-|}{\omega} (1 - \frac{\omega}{|\Omega^-|})^3$$

$$= \frac{B^2}{8\pi N} \frac{f_g}{f} (1 - \frac{f}{f_g})^3 . \qquad (5)$$

To calculate the growth rate, Kennel and Petschek [1966] considered $\omega = \omega_R + i\gamma$ where ω_R and γ were read and they assumed $\gamma/\omega_R \ll 1$. They evaluated the singular velocity integrals in Equation 1 using the Dirac relation:

$$\lim_{\gamma \to 0^+} \frac{1}{V_{||} - \frac{\omega - |\Omega^-|}{k}} = \frac{P}{V_{||} - \frac{\omega - |\Omega^-|}{k}} + i\pi(\text{sign } k)\, \delta\left(V_{||} - \frac{\omega - |\Omega^-|}{k}\right)$$

where P denoted the principal part. By equating real and imaginary parts in Equation 1 and by dropping terms of the order $(\gamma/\omega_R)^2$, they found ω_R was still given by Equation 3 and that the growth rate γ was

$$\gamma = \pi|\Omega^-|\left(1 - \frac{\omega}{|\Omega^-|}\right)^2 \eta(V_R) \cdot \left\{ A(V_R) - \frac{1}{\frac{|\Omega^-|}{\omega} - 1} \right\} \qquad (6)$$

where they defined

$$\eta(V_R) = 2\pi \frac{|\Omega^-| - \omega}{k} \cdot \int_0^\infty V_\perp \, dV_\perp \, F(V_\perp, V_{||} = V_R)$$

and

$$A(V_R) = \left. \frac{\int_0^\infty V_\perp \, dV_\perp \left(V_{||} \frac{\partial F}{\partial V_\perp} - V_\perp \frac{\partial F}{\partial V_{||}} \right) \frac{V_\perp}{V_{||}}}{2\int_0^\infty V_\perp \, dV_\perp \, F} \right|_{V_{||}=V_R}$$

$$= \left. \frac{\int_0^\infty V_\perp \, dV_\perp \tan\alpha \frac{\partial F}{\partial \alpha}}{2\int_0^\infty V_\perp \, dV_\perp \, F} \right|_{V_{||}=V_R}$$

where $\alpha = \tan^{-1}(-V_\perp/V_{||})$ was the pitch angle.

The above formalism developed by Kennel and Petschek [1966] has been quite useful in interpreting our observations. We have seen that whistler-mode wave growth has occurred when electrons with energies appropriate for cyclotron resonance have abrupt intensity enhancements. As predicted from Equation 6 the upper cutoff frequency of the wave spectrum is dependent on the anisotropy of the resonant electron pitch angle distributions. And we have observed wave damping or lack of wave growth when the resonant electrons have had flat or concave pitch angle distributions. However, it is somewhat cumbersome to do growth rate calculations using Equation 6 since the particle observations are usually presented as functions of energy and pitch angle, not perpendicular and parallel velocity distributions. For the growth rate calculations to follow we used a modified version of a numerical integration program developed by Sentman et al. [1976] which in turn was based on a growth rate expression obtained by Lerche [1967] who began his analysis with the relativistic Vlasov equation. It is appropriate to use the relativistic formulation because although the resonant energy for the cases we have been studying have been non-relativistic, contributions to wave growth or damping still come from higher energies which are near-relativisitic. We modified the Sentman et al. [1976] program to make it appropriate for higher frequency whistler-mode waves and low energy electrons. We also expanded it to handle non-parallel propagation and the resulting additional resonances. For non-parallel propagation the resonant

denominator in Equation 1 has the form

$$k_{||}V_{||}-\omega + m\Omega^- = k_{||}V_{||}-\omega - m\Omega$$

where $\Omega = |\Omega^-|$. For non-parallel propagation Kennel [1966] derived the following growth rate expression for whistler-mode waves:

$$\gamma = \pi^2 \Omega \frac{\omega}{k} \int_0^\infty V_\perp^2 \, dV_\perp \int_{-\infty}^{\infty} dV_{||} \sum_m \delta\left(V_{||} - \frac{\omega+m\Omega}{k_{||}}\right) \theta_m G_1 \qquad (7)$$

where θ_m the weighting function for a given resonance, m, is $\theta_m = \left\{ [(1 + \cos\theta) J_{m+1} + (1 - \cos\theta) J_{m-1}]/2 \cos\theta \right\}^2$. θ is the angle between the magnetic field and the wave normal direction. J_m is an ordinary Bessel function of integral order. The arguments of the Bessel functions are $k_\perp V_\perp/\Omega^-$. For strictly parallel propagation only the m = -1 resonance is non-zero.

$$G_1 = \frac{\partial F}{\partial V_\perp} - \frac{k_{||}}{\omega}\left(V_{||} \frac{\partial F}{\partial V_\perp} - V_\perp \frac{\partial F}{\partial V_{||}}\right) \qquad (8)$$

and must be evaluated at the appropriate resonance. For non-parallel propagation,

$$n^2 \approx \frac{(\omega_p^-)^2}{\omega(\Omega \cos\theta - \omega)} .$$

Using this dispersion relation one finds that for the cyclotron resonances ($m \neq 0$),

$$E_R \approx m^2 \frac{B^2}{8\pi N \cos\theta} \left(1 + \frac{\omega}{m\Omega}\right)^2 \left(\frac{\Omega}{\omega} - \frac{1}{\cos\theta}\right)$$

and that for the Landau resonance (m = 0)

$$E_L \approx \frac{\omega}{\Omega} \frac{B^2}{8\pi N \cos\theta} \left(1 - \frac{\omega}{\Omega \cos\theta}\right)$$

For our growth rate calculations we used the weighting function derived by Kennel [1966] but used the exact dispersion relation, Equation 1-26 in Stix [1962]. As will be shown, the results of our growth rate calculations are consistent with the Kennel and Petschek [1966] growth rate expressions, especially the upper frequency cutoff as a function of the pitch angle anisotropy of the resonant electrons.

B. Results of the Growth Rate Calculations

Panel (a) of Figure 23 shows the calculated growth rates based on the observed electron energy spectra and pitch angle distributions for inbound L = 5.2 (~ 1040 UT) for Orbit 35 which was prior to the anisotropic low energy electron enhancement discussed in Section IV-A. Panel (b) of Figure 23 shows the calculated growth rates for inbound L = 4.9 (~ 1130 UT) for Orbit 35 which was during the anisotropic low energy enhancement. $N = 10\ cm^{-3}$ was used for both growth rate calculations but f_g was adjusted according to the measured magnetic field. Since wave amplitude is proportional to $e^{\gamma t}$, the higher γ's correspond to very large increases in wave amplitude. The total growth and corresponding wave amplitudes depend on how much time the wave spends in the interaction region. This in turn is dependent on

the group velocity of the wave and the size of the interaction region.

These growth rate calculations indicate that prior to the anisotropic electron enhancement only very weak wave growth up to $\sim 0.3\ f_g$ could be supported by the observed electron distributions. In the observed electric field data no strong bands of chorus were evident prior to the electron enhancement. The growth rate calculations for 1130 UT indicate strong wave growth from $\sim 0.29\ f_g$ to $\sim 0.55\ f_g$. And in the wideband analog data in Figure 8 around 1130 UT strong bands of chorus are present in the frequency range from 2.0 kHz to 3.0 kHz which corresponds to $0.35\ f_g$ to $0.53\ f_g$. This comparison between the calculated growth rate and the wideband analog data shows that the observed wave spectra could be produced by wave amplification via the electron cyclotron resonant interaction during the period of enhanced low energy electron flux.

In addition to showing the calculated growth rate of parallel propagating waves ($\theta = 0°$) for the $n = -1$ electron cyclotron resonance, we have also plotted in panel (b) the growth rates for the $m = 1$ resonance at $\theta = 10°$, $20°$ and $30°$ and the Landau resonance ($m = 0$) damping rate for $\theta = 10°$. Higher negative and positive resonance have not been shown because they are much weaker. Since the energy spectra decrease exponentially with increasing energy and the resonant energy increases as the order of the resonance increases, the higher order resonances have little effect on the growth rate, especially at small wave normal angles. The growth rate curves in panel (b) show

that the positive growth rate decreases and the damping increases as the wave normal angle increases.

Figure 24 shows the calculated growth rates for ~ 1856 UT on orbit 36 during the very anisotropic electron enhancement discussed in Section IV-B. For this calculation we used N = 8 cm^{-3}. The calculation shows weak growth up to ~ 0.3 f_g and then negative growth (damping) up to 0.51 f_g. Strong growth is then produced up to 0.6 f_g. We have assumed N = 8 cm^{-3} because at N = 7 cm^{-3} and below the calculated growth rates show growth only below 0.3 f_g. As N is increased above 8 cm^{-3}, the strong growth begins at values below 0.5 f_g contrary to the wideband observations shown in Figure 15. When the very anisotropic portion of the electron distribution was replaced with a milder distribution proportional to $\sin^2 \alpha$, while the electron intensities were unchanged the calculations showed no growth above 0.5 f_g. This implies that the intense wave spectra observed above 0.5 f_g is a result of wave amplification by the very anisotropic electrons.

Figure 25 shows the calculated growth rate for the half-gyrofrequency whistler-mode noise discussed in Section IV-D for Orbit 36. Strong growth is predicted from 0.25 f_g up to 0.63 f_g. This range includes the location of the observed peak intensities at 0.54 f_g and 0.58 f_g. When the half-gyrofrequency noise has been observed in the wideband analog data the observed frequency limits were ~ 0.3 f_g to ~ 0.6 f_g, consistent with these growth rate calculations.

VII. COMPARISON OF THE OBSERVED AND PREDICTED CHARACTERISTICS OF THE ELECTROSTATIC $f > f_g$ EMISSIONS

Young et al. [1973] and Ashour-Abdalla and Kennel [1975] found that electrostatic $f > f_g$ emissions in the magnetosphere required a background of cold electrons plus a warm electron species that has an anomalous perpendicular velocity distribution, i.e., the peak in the warm electron perpendicular velocity distribution occurs at $V_\perp \neq 0$. Such anomalous perpendicular velocity distributions for very low energy electrons have been observed in the plasma sheet [DeForest and McIlwain, 1971; Shield and Frank, 1970] from about 100 eV up to a few keV. We have not observed such anomalous electron distributions on S^3-A in conjunction with any of the electrostatic emissions we have investigated probably because they are below the 1.0 keV low energy cutoff of the electron detectors. However the very anistoropic 1.2 keV electrons observed in conjunction with the electrostatic emissions are an indication an anomalous distribution could exist at lower energies. The ambient background plasma in the magnetosphere outside the plasmasphere is cold and has a very low number density.

Both Young et al. [1973] and Ashour-Abdalla and Kennel [1975] found that the unstable frequency band for the electrostatic emissions depended only on the cold to hot density and on the ratio of the cold UHR frequency to the electron gyrofrequency. In all cases they found

that the growth rate peaked near but below the cold UHR frequency. Ashour-Abdalla and Kennel [1975] also found that the group velocity parallel to the magnetic field could have zeroes near the odd half-harmonics of the electron gyrofrequency, suggesting that the instabilities could be non-convective under certain conditions. Since their growth rate calculations indicate that all frequencies between the low-frequency cutoff and the UHR frequency should be unstable, the non-convective property could account for the bands of emissions near the odd half-harmonics of the gyrofrequency.

The dependence of the lower and upper frequency limits, $X_{min} = f_{min}/f_g$ and $X_{max} = f_{max}/f_g$, on the hot and cold number densities, N_H and N_C, is as follows: If N_H is kept fixed, increasing N_C increases both X_{min} and X_{max}. With N_H fixed, if N_C approaches zero, the range of unstable frequencies shrinks to zero. If N_C is kept fixed, increasing N_H decreases X_{min} but leaves X_{max} fixed. Waves nearly perpendicular to the ambient magnetic field have a lower X_{min} than waves more nearly parallel to the ambient magnetic field.

The above theoretical studies suggest that in the evening magnetosphere the electrostatic $f > f_g$ emissions are generated during geomagnetically disturbed times when very low energy electrons with an anomalous perpendicular velocity distribution are convected into the magnetosphere where they encounter a cold low number density background of electrons. The frequency bands of the electrostatic emissions are determined by the relative number densities of the two species. As the ratio of these two densities charge, the frequency

limits of the emissions change. This would account for the observed frequency changes in the wideband analog data.

VIII. DISCUSSION AND SUMMARY

This study has shown that chorus and other whistler-mode emissions and electrostatic $f > f_g$ emissions observed in the magnetosphere are associated with enhanced intensities of low energy electrons convected into the dusk to midnight sector of the magnetosphere from the plasma sheet during geomagnetically disturbed periods. Strong and continuous bands of chorus are observed only outside the plasmasphere and then only when large fluxes of anisotropic low energy electrons at energies appropriate for cyclotron resonance with the chorus waves are present. For strong chorus emissions to be observed, the differential directional intensities of 1-10 keV electrons must of the order of 10^7 to 10^8 electrons $(cm^2 \text{ sec ster keV})^{-1}$. Using the estimated number density and the measured gyrofrequency we have shown that the enhanced electron intensities occur for energies that are appropriate for cyclotron resonance with the chorus waves. The chorus amplitudes tended to be higher the greater the flux of resonant electrons.

By comparing the spectra of the whistler-mode emissions and the pitch angle distributions of the resonant electrons we have shown that in agreement with the predictions of Kennel and Petschek [1966], the upper frequency cutoff of the chorus spectra is dependent on the anisotropy of the resonant electrons. The greater the anisotropy,

the larger the upper cutoff frequency of the chorus will be. An example of wave damping when the anisotropy of the resonant electrons was negative has also been presented.

Growth rate calculations using the observed electron energy spectra and pitch angle distributions showed that the calculated frequency limits of the whistler-mode spectra are in good agreement with the observed spectra. However, the growth rate calculations have not been able to produce the band of "missing emissions" near $f_g/2$ observed in the chorus spectra. Tsurutani and Smith [1974] suggested that a possible explanation for the missing band might be Landau damping. For electrons in cyclotron resonance with waves at $f = f_g/2$, the parallel velocity of the electrons equals the wave phase velocity but the electrons are moving in the opposite direction. Assuming that the electrons are moving along the field not bunched and in both directions, they noted that there would be electrons also moving in the same direction as the wave and with a velocity equal to the wave phase velocity. These electrons will Landau damp the wave provided they lie on a portion of the particle distribution function that is decreasing with energy. The problem with this explanation is that strictly parallel propagating waves do not Landau damp. Landau damping is significant only for waves with large wave normal angles.

Another possible explanation for the missing emission band that considers separate sources for the $f < f_g/2$ and $f > f_g/2$ waves has been proposed by Maeda et al. [1976]. They suggest that the $f > f_g/2$ emissions might be generated locally near the satellite while the

$f < f_g/2$ emissions are generated in a similar way but slightly outside the observing location where the local electron gyrofrequency would be lower. When these lower frequency emissions ultimately propagate to the observing location via the ducted mode, their upper frequency cutoff will be one half the equatorial gyrofrequency of the observing location. However, these waves would be expected to be propagating nearly parallel to the magnetic field and thus their electric field should be spin modulated. We have found no evidence of this spin modulation.

A third possible explanation is that the source spectra of the original whistler-mode wave has a band of missing emissions near $f_g/2$. The cyclotron resonant wave interaction process does not "generate" waves but rather amplifies low amplitude waves. If the source spectra were void of a band near $f_g/2$, the amplified waves would also be void of this same band.

Since we have been able to nearly duplicate the observed whistler-mode spectra in the growth rate calculations using the observed electron gyrofrequency and electron energy spectra and pitch angle distributions and adjusting the number density, this procedure could be used to determine the number density. The growth rate calculations are quite sensitive to number density especially when the number density is low.

This study has shown that electrostatic emissions that can occur in several bands from slightly above f_g up to the UHR frequency are associated with very low energy electrons ($E \leq 1$ keV). The

emissions near $3f_g/2$ are observed to be propagating nearly perpendicular to the ambient magnetic field. Throughout an orbit the frequency limits of the electrostatic bands often change. On one occasion the change in frequency limits occurred quasi-periodically with a period roughly equivalent to that of a PC3 micropulsation event observed at a ground station at the same time. These observations are in agreement with the theory of generation of magnetospheric electrostatic emissions that predicts the frequency limits are determined by the hot and cold electron number densities. In order to improve our observations we require rapid temporal measurements of electron spectra and pitch angle distributions for electrons with energies well below 1 keV. We also need precise rapid measurements of the ambient electron number density. Only then can the theory be truly verified.

REFERENCES

Anderson, R. R. and D. A. Gurnett, Plasma wave observations near the plasmapause with the S^3-A satellite, J. Geophys. Res., 78, 4756-4764, 1973.

Ashour-Abdalla, M. and C. F. Kennel, VLF electrostatic waves in the magnetosphere, in Physics of the Hot Plasma in the Magnetosphere, B. Hultqvist and L. Stenflow, Eds., pp. 201-227, Plenum, New York, 1975.

Barrington, R. E., T. R. Hartz, and R. W. Harvey, Diurnal distribution of ELF, VLF, and LF noise at high latitudes as observed by Alouette 2, J. Geophys. Res., 76, 5278-5291, 1971.

Burtis, W. J. and R. A. Helliwell, Banded chorus - a new type of VLF radiation observed in the magnetosphere by OGO 1 and OGO 3, J. Geophys. Res., 74, 3002-3010, 1969.

Burton, R. K. and R. E. Holzer, The origin and propagation of chorus in the outer magnetosphere, J. Geophys. Res., 79, 1014-1023, 1974.

Carpenter, D. L., Whistler studies of the plasmapause in the magnetosphere, 1. Temporal variations in the position of the knee and some evidence on plasma motions near the knee, J. Geophys. Res., 71, 693-709, 1966.

De Forest, S. E. and C. E. McIlwain, Plasma clouds in the magnetosphere, J. Geophys. Res., 76, 3587-3611, 1971.

Dunckel, N. and R. A. Helliwell, Whistler-mode emissions on the OGO 1 satellite, J. Geophys. Res., 74, 6371-6385, 1969.

Fredricks, R. W., Wave-particle interactions in the outer magnetosphere: a review, in The Magnetospheres of the Earth and Jupiter, V. Formisano, Ed., pp. 113-152, D. Reidel Publishing Company, Dordrecht-Holland, 1975.

Fredricks, R. W. and F. L. Scarf, Recent studies of magnetospheric electric field emissions above the electron gyrofrequency, J. Geophys. Res., 78, 310-314, 1973.

Gurnett, D. A. and R. R. Shaw, Electromagnetic radiation trapped in the magnetosphere above the plasma frequency, J. Geophys. Res., 78, 8136-8149, 1973.

Kennel, C., Low-frequency whistler mode, Phys. Fluids, 9, 2190-2202, 1966.

Kennel, C. F. and H. E. Petschek, Limit on stably trapped particle fluxes, J. Geophys. Res., 71, 1-28, 1966.

Kennel, C. F., F. L. Scarf, R. W. Fredricks, J. H. McGehee, and F. V. Coroniti, VLF electric field observations in the magnetosphere, J. Geophys. Res., 75, 6136-6152, 1970.

Lerche, I., Unstable magnetosonic waves in a relativistic plasma, Astrophys. J., 147, 689-696, 1967.

Longanecker, G. W. and R. A. Hoffman, S^3-A spacecraft and experiment description, J. Geophys. Res., 78, 4711-4717, 1973.

Lyons, L. R. and D. J. Williams, The quiet time structure of energetic (35-560 keV) radiation belt electrons, J. Geophys. Res., 80, 943-950, 1975.

Maeda, K., P. H. Smith, and R. R. Anderson, VLF-emissions from ring current electrons, submitted for publication, Nature, 1976.

Morgan, M. G. and N. C. Maynard, Evidence of dayside plasmaspheric structure through comparisons of ground-based whistler data and Explorer 45 plasmapause data, J. Geophys. Res., 81, 3992-3998, 1976.

Oliven, M. N. and D. A. Gurnett, Microburst phenomena, 3. An association between microbursts and VLF chorus, J. Geophys. Res., 73, 2355-2362, 1968.

Parady, B. and L. J. Cahill, Jr., ELF observations during the December 1971 storm, J. Geophys. Res., 78, 4765-4770, 1973.

Rosenberg, T. J., R. A. Helliwell, and J. P. Katsufrakis, Electron precipitation associated with discrete very-low-frequency emissions, J. Geophys. Res., 76, 8445-8452, 1971.

Russell, C. T., R. E. Holzer, and E. J. Smith, OGO 3 observations of ELF noise in the magnetosphere, 1. Spatial extent and frequency of occurrence, J. Geophys. Res., 74, 755-777, 1969.

Scarf, F. L., R. W. Fredricks, C. F. Kennel, and F. V. Coroniti, Satellite studies of magnetospheric substorms on August 15, 1968, J. Geophys. Res., 78, 3119-3130, 1973.

Schield, M. A. and L. A. Frank, Electron observations between the inner edge of the plasma sheet and the plasmasphere, J. Geophys. Res., 75, 5401-5414, 1970.

Sentman, D. D., C. K. Goertz, and J. A. Van Allen, Cold plasma densities from energetic electron pitch angle distributions in the inner Jovian magnetosphere, submitted for publication, Geophysical Research Letters, 1976.

Shaw, R. R. and D. A. Gurnett, Electrostatic noise bands associated with the electron gyrofrequency and plasma frequency in the outer magnetosphere, J. Geophys. Res., 80, 4259-4271, 1975.

Stix, T. H., The Theory of Plasma Waves, McGraw-Hill, New York, 12, 1962.

Sugiura, M. and D. J. Poros, Dst for 1971 and 1972, NASA-Goddard Space Flight Center, Greenbelt, MD 20771, April, 1973.

Taylor, W. W. L. and D. A. Gurnett, Morphology of VLF emissions observed with the Injun 3 satellite, J. Geophys. Res., 73, 5615-5626, 1968.

Tsurutani, B. T. and E. J. Smith, Postmidnight chorus: a substorm phenomenon, J. Geophys. Res., 79, 118-127, 1974.

Williams, D. J., J. N. Barfield, and T. A. Fritz, Initial Explorer 45 substorm observations and electric field considerations, J. Geophys. Res., 79, 554-564, 1974.

Young, T. S. T., J. D. Callen, and J. E. McCune, High-frequency electrostatic waves in the magnetosphere, J. Geophys. Res., 78, 1082-1099, 1973.

APPENDIX A

TABLES

Table 1

S^3-A Electron Channeltron and Solid State Electron Detector Energy Bands

Level Designation	Mean Energy (keV)	ΔE (keV)
E2	1.37	0.36
E4	1.76	0.55
E6	2.69	0.83
E8	4.04	1.26
E10	6.04	1.88
E12	9.16	2.84
E14	13.50	4.19
E16	25.62	7.94
SSED1	55.0	35.0
SSED2	100.0	50.0
SSED3	180.0	120.0
SSED4	400.0	320.0

APPENDIX B

FIGURES

Figure 1 Expanded time scale frequency-time spectrograms of wideband analog data which contain bands of chorus. The top panel of each set contains data from the search coil magnetometer experiment and the bottom panel of each set contains data from the electric field experiment. The calibration marks for these spectrograms occur at one minute intervals and are 1 kHz apart in frequency. The measured local electron gyrofrequency, f_g, and $f_g/2$ are indicated at the right side of each spectrogram. The chorus bands appear more intense in the electric field data than in the magnetic field data because the electric field receiver has more sensitivity and a wider dynamic range. Note that the chorus bands usually display a band of "missing emissions" near $f_g/2$.

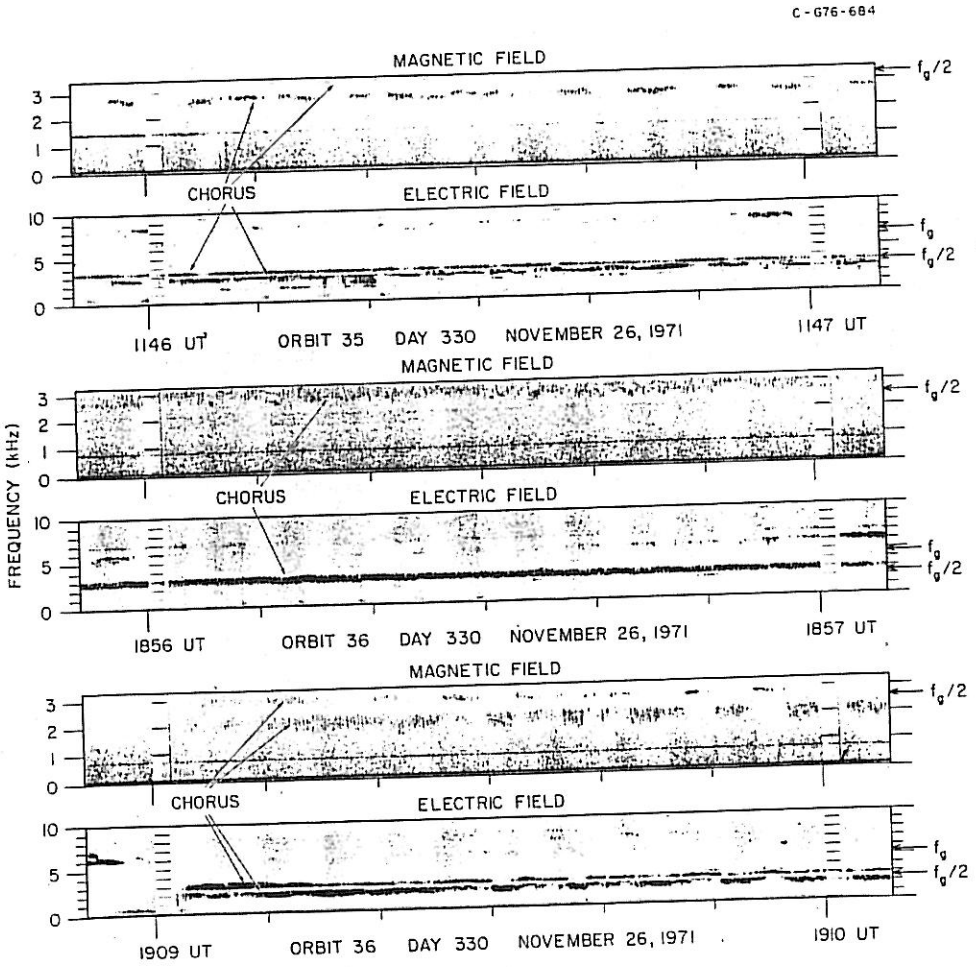
C-G76-684
MAGNETIC FIELD
$f_g/2$
CHORUS
ELECTRIC FIELD
f_g
$f_g/2$
1146 UT
ORBIT 35 DAY 330 NOVEMBER 26, 1971
1147 UT
MAGNETIC FIELD
$f_g/2$
FREQUENCY (kHz)
CHORUS
ELECTRIC FIELD
f_g
$f_g/2$
1856 UT
ORBIT 36 DAY 330 NOVEMBER 26, 1971
1857 UT
MAGNETIC FIELD
$f_g/2$
CHORUS
ELECTRIC FIELD
f_g
$f_g/2$
1909 UT
ORBIT 36 DAY 330 NOVEMBER 26, 1971
1910 UT

Figure 1

Figure 2 A one hour frequency-time spectrogram of the electric field wideband analog data for Orbit 115 on December 22, 1971. The integral half harmonics of the electron gyrofrequency are plotted on the spectrogram as fenced lines. Chorus bands with the missing emission band near $f_g/2$ are clearly evident in the lower portion of the spectrogram. Several bands of electrostatic emissions are evident in the top portion. Their frequency limits extend from just above f_g to above $3f_g/2$.

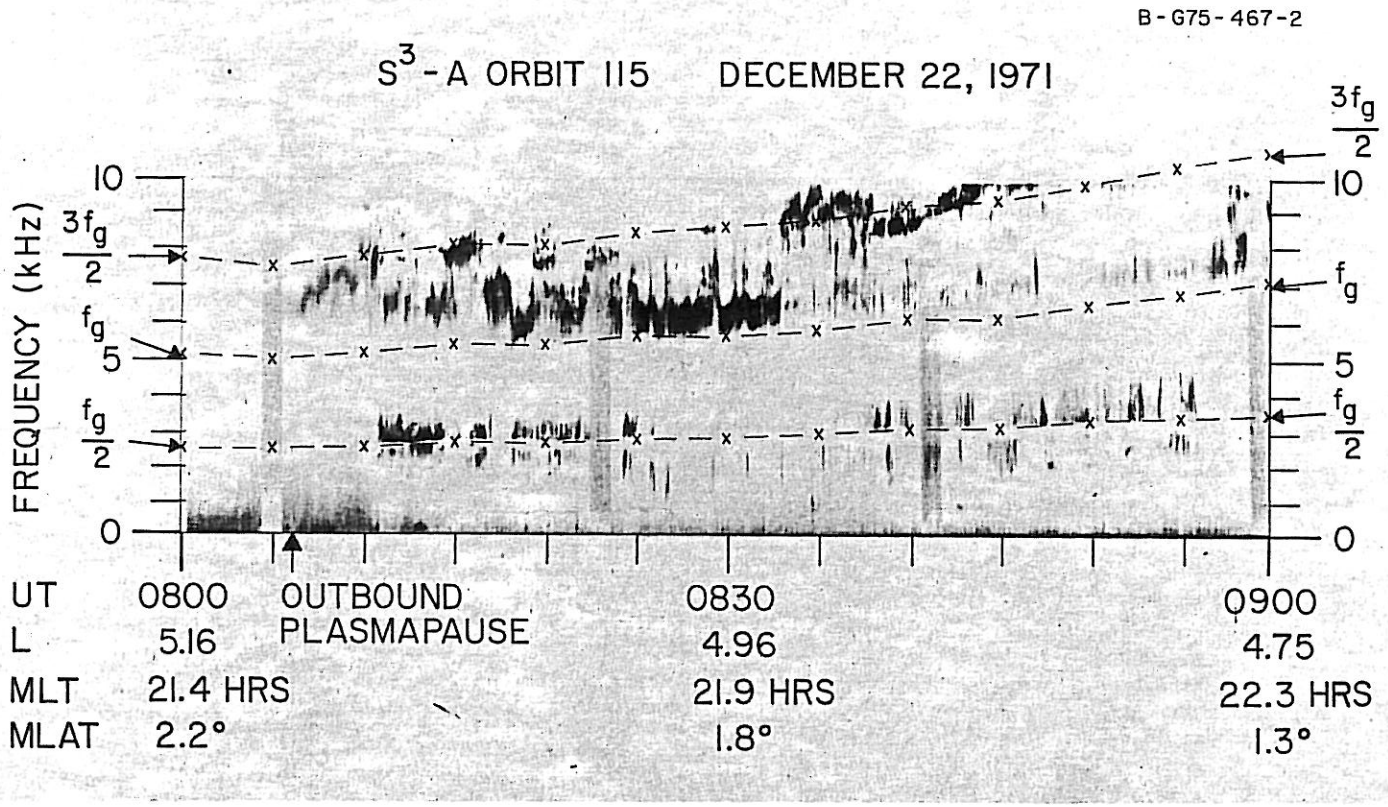
B-G75-467-2
S3-A ORBIT 115 DECEMBER 22, 1971
FREQUENCY (kHz)
10
3fg/2
fg
5
fg/2
0
3fg/2
10
fg
5
fg/2
0
UT 0800 OUTBOUND PLASMAPAUSE 0830 0900
L 5.16 4.96 4.75
MLT 21.4 HRS 21.9 HRS 22.3 HRS
MLAT 2.2° 1.8° 1.3°

Figure 2

Figure 3 Expanded time scale frequency-time spectrograms of electric field wideband analog data which contain electrostatic $f > f_g$ emissions. The calibration marks for these spectrograms occur at one minute intervals and are 1 kHz apart in frequency. The measured local electron gyrofrequency is indicated at the right side of each spectrogram. The electrostatic emissions occur in several bands and the frequency limits of these bands can range from f_g to $2f_g$. The arrows at the top of each spectrogram indicate when the axis of the electric dipole antenna is most nearly aligned parallel to the ambient magnetic field. The nulls in the emission bands occur very close to when the electric dipole antenna is most nearly aligned parallel to the ambient magnetic field. This indicates the electrostatic emissions are propagating nearly perpendicular to the ambient magnetic field.

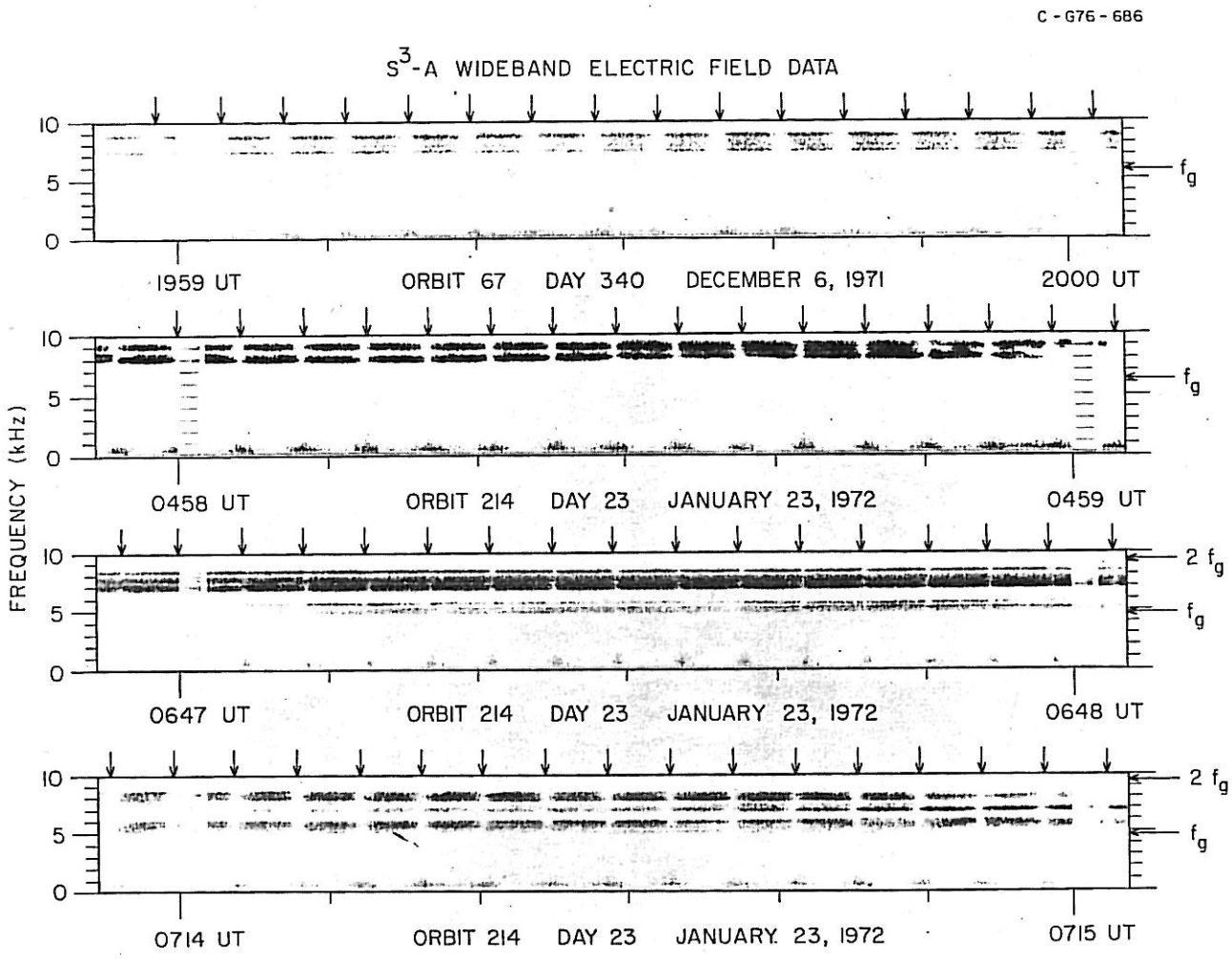
C - G76 - 686
S3-A WIDEBAND ELECTRIC FIELD DATA
FREQUENCY (kHz)
10
5
0
fg
1959 UT
ORBIT 67 DAY 340 DECEMBER 6, 1971
2000 UT
0458 UT
ORBIT 214 DAY 23 JANUARY 23, 1972
0459 UT
2 fg
0647 UT
0648 UT
0714 UT
0715 UT
JANUARY 23, 1972

Figure 3

Figure 4 Frequency-time spectrograms of wideband analog data for Orbit 101 on December 17, 1971. The top spectrogram contains the magnetic field data and the bottom spectrogram contains the electric field data. In addition to the orbit parameters L, Magnetic Local Time and Magnetic Latitude, the label below the spectrograms also includes the measured local electron gyrofrequency at ten minute intervals. Chorus is present in both the magnetic and electric field spectrograms. The electrostatic $f > f_g$ emissions are present only in the electric field data even when f_g drops to $\sim$ 2.2 kHz near 1950 UT and the electrostatic emissions occur below the 3 kHz upper frequency cutoff of the search coil magnetometers. This confirms that the $f > f_g$ emissions are primarily electrostatic.

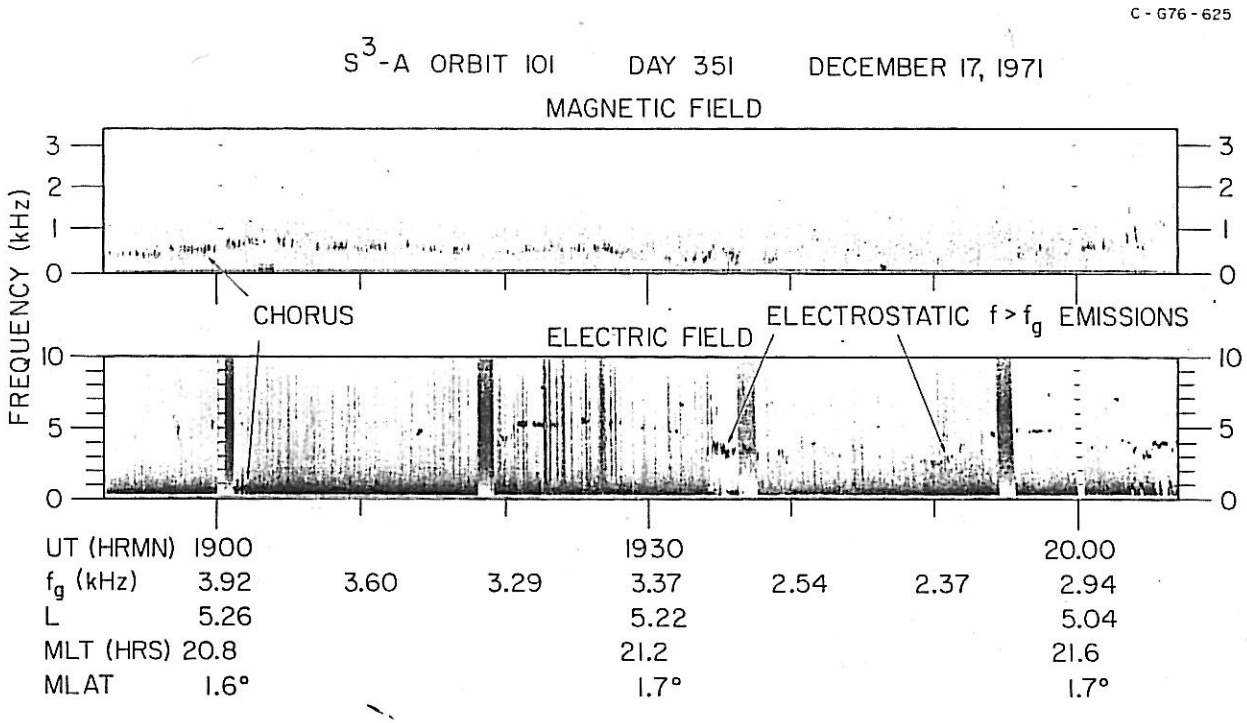
C - G76 - 625
S3-A ORBIT 101 DAY 351 DECEMBER 17, 1971
MAGNETIC FIELD
FREQUENCY (kHz)
3
2
1
0
CHORUS
ELECTRIC FIELD
ELECTROSTATIC f > fg EMISSIONS
10
5
0
UT (HRMN) 1900 1930 20.00
fg (kHz) 3.92 3.60 3.29 3.37 2.54 2.37 2.94
L 5.26 5.22 5.04
MLT (HRS) 20.8 21.2 21.6
MLAT 1.6° 1.7° 1.7°

Figure 4

Figure 5 Frequency-time spectrogram of the electric field wideband analog data for Orbit 214 on January 23, 1972. The electrostatic $f > f_g$ emissions are present as bands throughout the period the satellite is outside the plasmasphere until they exceed the 10 kHz upper frequency cutoff of the wideband receiver. Near apogee the strongest bands are between 1.5 and 2.0 f_g while at lower altitudes the strongest bands were between 1.0 and 1.5 f_g. This is in contrast to the electrostatic emissions observed for Orbit 115 and shown in Figure 2 where the strongest electrostatic emissions were between 1.0 and 1.5 f_g near apogee but were near or above 1.5 f_g at lower altitudes. As discussed later in the text, the frequency limits of the electrostatic emissions are determined by the number densities of the hot and cold electrons.

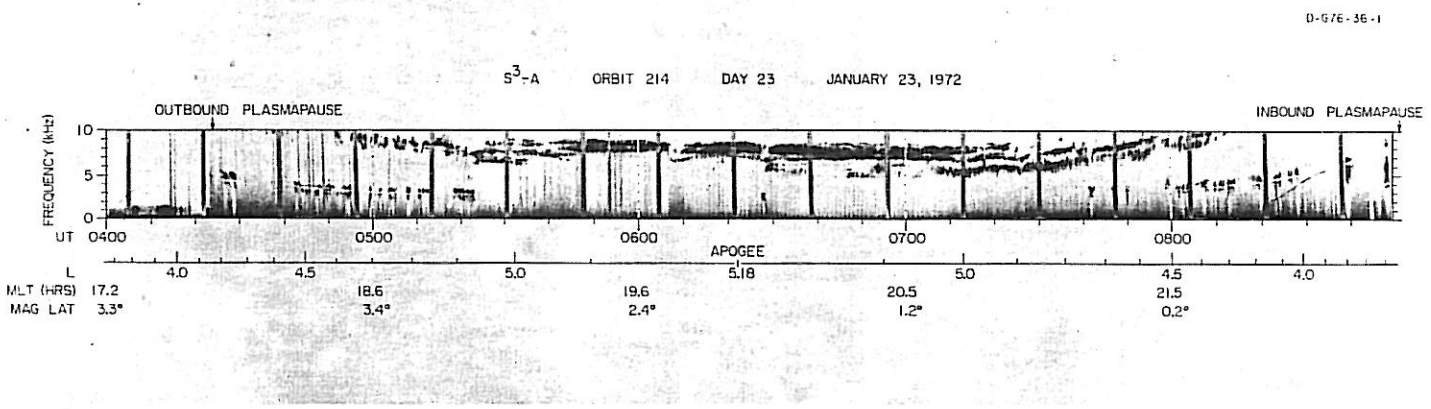
D-G76-36-1
S3-A ORBIT 214 DAY 23 JANUARY 23, 1972
OUTBOUND PLASMAPAUSE
INBOUND PLASMAPAUSE
FREQUENCY (kHz)
10
5
0
UT 0400 0500 0600 0700 0800
APOGEE
L 4.0 4.5 5.0 5.18 5.0 4.5 4.0
MLT (HRS) 17.2 18.6 19.6 20.5 21.5
MAG LAT 3.3° 3.4° 2.4° 1.2° 0.2°

Figure 5

Figure 6 A plot of the digital output from the 16 channel onboard spectrum analyzer for the entire Orbit 214. The bottom channel is wideband and covers the frequency range from 0.1 to 10.0 kHz and the remaining 15 narrowband channels have center frequencies from 35 Hz to 100 kHz. The output level of each channel is approximately linearly proportional to the logarithm of the measured amplitude. The vertical lines represent the average amplitude measured over 64 second intervals of time and the dots are peak amplitudes over the same time period. The baseline for each channel is about 2 $\mu V\ m^{-1}$ and full scale is about 20 $mV\ m^{-1}$. PP indicates the plasmapause locations. The dashed line labeled f_p indicates the location of the electron plasma frequency as determined from the UHR noise. The dashed lines labeled f_g and $2f_g$ indicate the location of the first and second harmonics of the electron gyrofrequency. Note that near apogee the electrostatic noise extends as high as 31.1 kHz which corresponds to $\sim 11 f_g/2$.

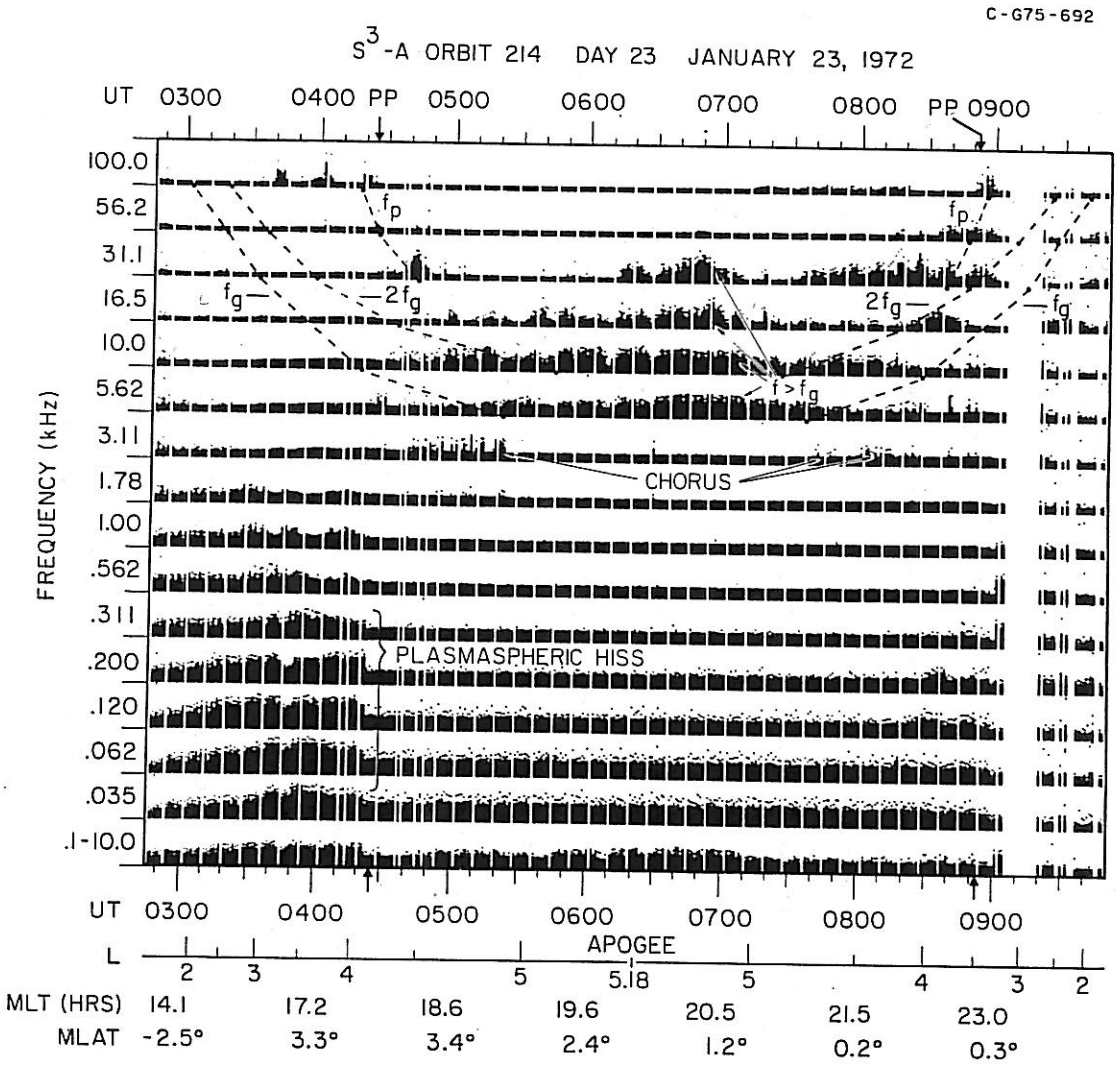
C-G75-692
S3-A ORBIT 214 DAY 23 JANUARY 23, 1972
UT 0300 0400 PP 0500 0600 0700 0800 PP 0900
100.0
56.2
31.1
16.5
10.0
5.62
3.11
1.78
1.00
.562
.311
.200
.120
.062
.035
.1-10.0
FREQUENCY (kHz)
fp
fg
2fg
f>fg
CHORUS
PLASMASPHERIC HISS
UT 0300 0400 0500 0600 0700 0800 0900
APOGEE
L 2 3 4 5 5.18 5 4 3 2
MLT (HRS) 14.1 17.2 18.6 19.6 20.5 21.5 23.0
MLAT -2.5° 3.3° 3.4° 2.4° 1.2° 0.2° 0.3°

Figure 6

Figure 7 Electron intensity plots and electric field digital spectrum analyzer data for Orbit 35 on November 26, 1971. The top portion contains plots of the differential directional electron intensity, electrons $(cm^2$ sec ster keV$)^{-1}$, at $\alpha \sim 90°$ for electrons with mean energies from 1.2 keV to 100.0 keV for the entire orbit. The bottom portion displays the electric field digital spectrum analyzer output from 1.0 kHz to 100.0 kHz for the same time period. The measured electron gyrofrequency, f_g, has been drawn in as a dashed line. PP indicates the plasmapause locations. The shaded area on the electron plots bounded by vertical dashed lines highlights the enhanced low energy electron intensities. Note that the strong continuous bands of chorus and the electrostatic $f > f_g$ emissions occur only during the time of the enhanced low energy electron intensities. The sporadic bursts of chorus prior to this enhancement are a result of the relatively high background intensities of the low energy electrons.

D-G76-545

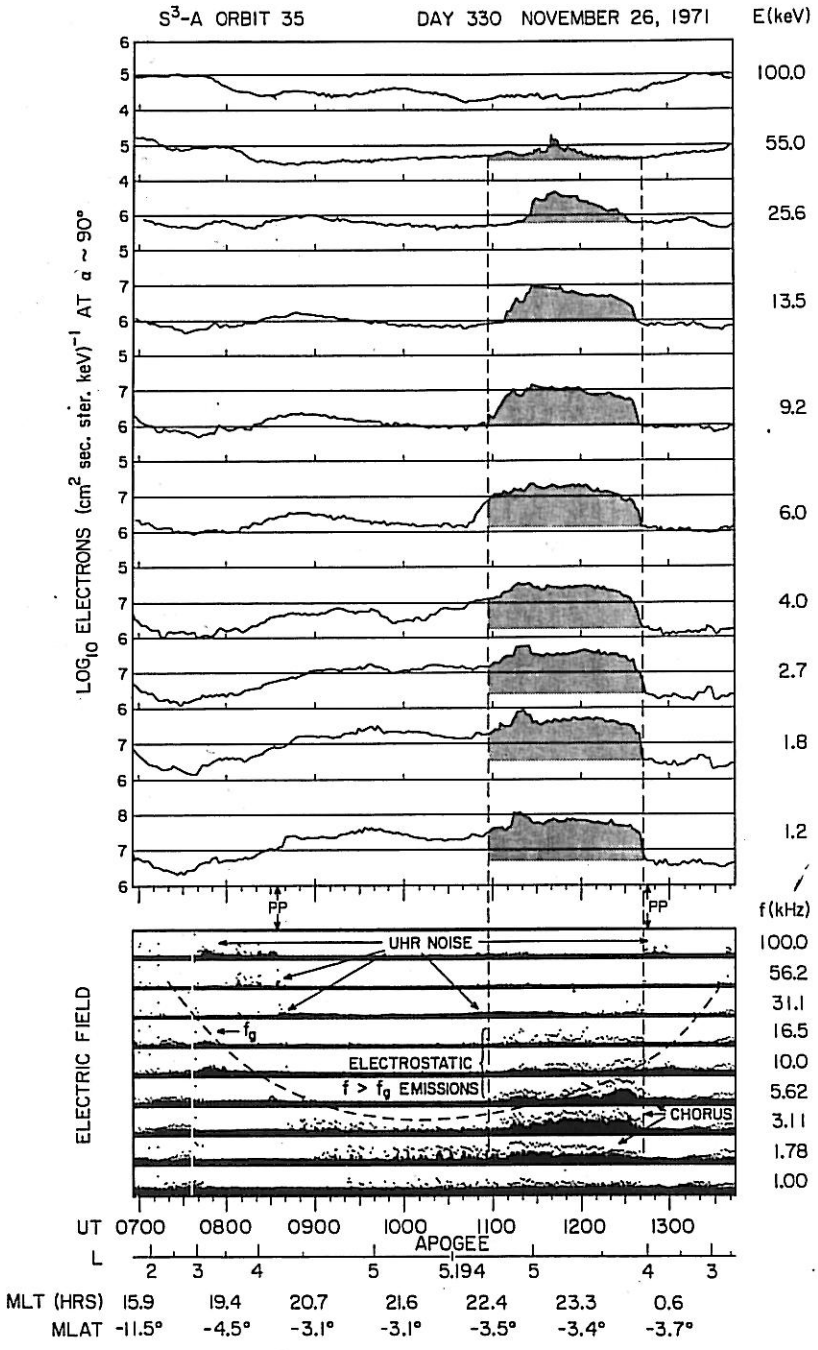

Figure 7

Figure 8 Frequency-time spectrograms of the search coil magnetometer and electric field wideband analog data during the time of the enhanced low energy electron intensities for Orbit 35. The measured local electron gyrofrequency at ten minute intervals is indicated in the label below the spectrograms. The most intense chorus bands lie between $\sim 0.4\ f_g$ and $\sim 0.6\ f_g$ but near the inbound plasmapause crossing the chorus bands extend down to $\sim 0.25\ f_g$. A relatively weak electrostatic emission band above f_g is evident for the first hour until it exceeds the 10 kHz upper frequency limit of the wideband electric field receiver.

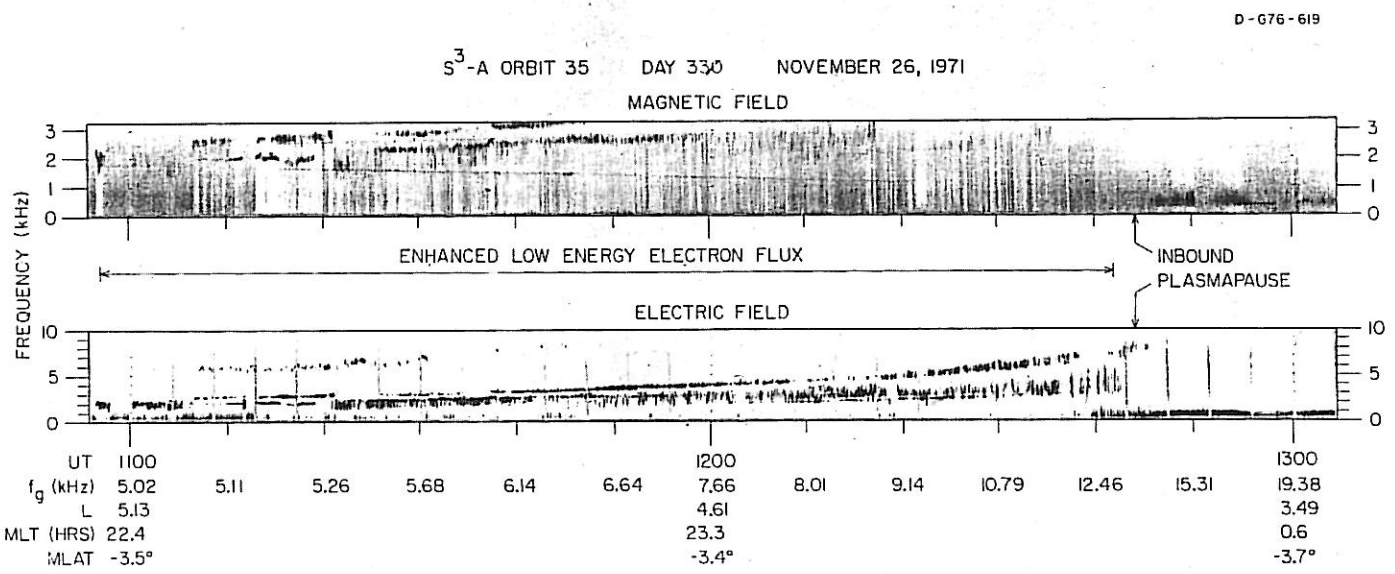
D-G76-619
S3-A ORBIT 35 DAY 330 NOVEMBER 26, 1971
MAGNETIC FIELD
FREQUENCY (kHz)
3
2
1
0
ENHANCED LOW ENERGY ELECTRON FLUX
INBOUND
PLASMAPAUSE
ELECTRIC FIELD
10
5
0
UT 1100 1200 1300
fg (kHz) 5.02 5.11 5.26 5.68 6.14 6.64 7.66 8.01 9.14 10.79 12.46 15.31 19.38
L 5.13 4.61 3.49
MLT (HRS) 22.4 23.3 0.6
MLAT -3.5° -3.4° -3.7°

Figure 8

Figure 9 A plot of equatorial D_{st} from November 17 to November 30, 1971. S^3-A Orbits 35 and 36 occurred about a day after geomagnetic disturbances which had been active for nearly a week reached peak intensity and slowly began to subside.

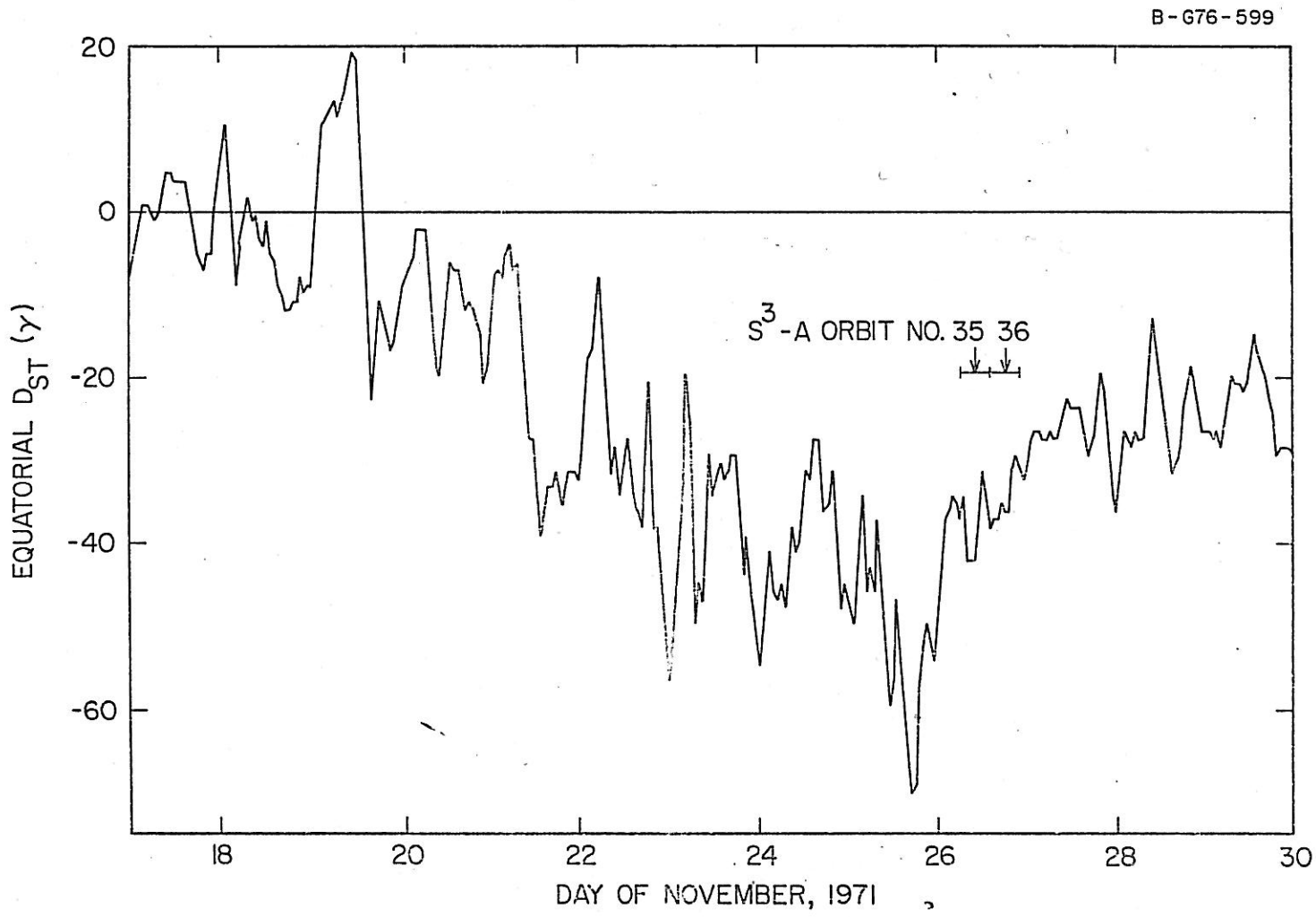
B-G76-599
20
0
-20
-40
-60
EQUATORIAL D_{ST} (γ)
S^3-A ORBIT NO. 35 36
18
20
22
24
26
28
30
DAY OF NOVEMBER, 1971

Figure 9

Figure 10 Differential directional intensity of electrons with pitch angle $\alpha \sim 90°$ at L = 5 for Orbit 35. The outbound L = 5 spectra is plotted as x's and the inbound L = 5 spectra is plotted as closed circles. The shaded area indicates the amount the inbound low energy electron intensity is enhanced over the outbound L = 5 levels. Also shown and plotted as closed squares is the mean quiet time spectra at L = 5.2 for Orbits 75-97 on December 9-16, 1971, from Lyons and Williams [1975]. The error bars indicate the maximum and minimum intensities observed for those orbits. Even the Orbit 35 L = 5 outbound intensities are elevated well above the mean quiet time levels. This accounts for the sporadic chorus bursts observed in the electric field spectrum analyzer data in Figure 7.

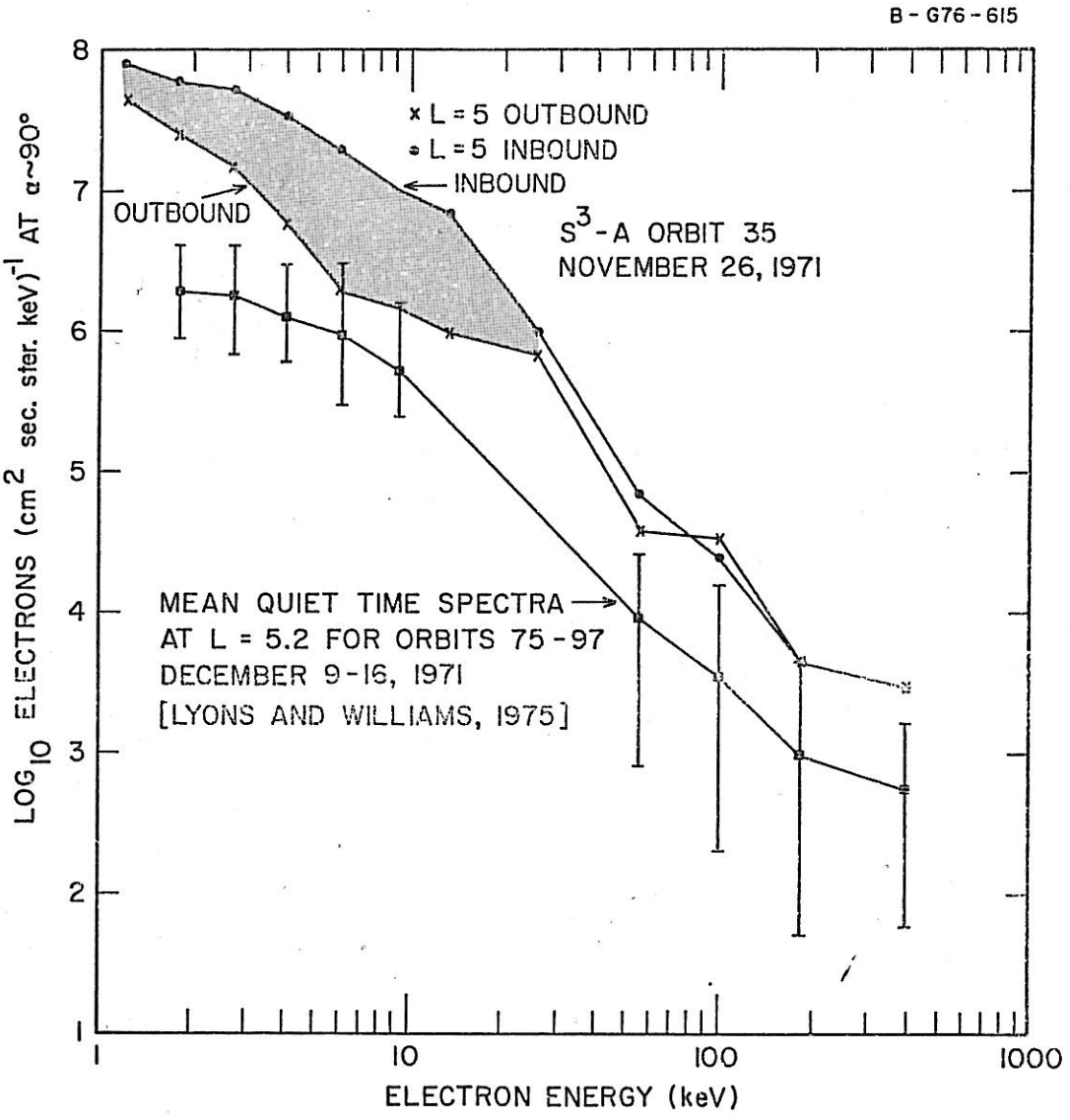
B - G76 - 615
× L = 5 OUTBOUND
• L = 5 INBOUND
← INBOUND
OUTBOUND
S3 - A ORBIT 35
NOVEMBER 26, 1971
MEAN QUIET TIME SPECTRA →
AT L = 5.2 FOR ORBITS 75 - 97
DECEMBER 9 - 16, 1971
[LYONS AND WILLIAMS, 1975]
LOG10 ELECTRONS (cm2 sec. ster. keV)-1 AT α~90°
ELECTRON ENERGY (keV)
1
2
3
4
5
6
7
8
1
10
100
1000

Figure 10

Figure 11 Electron intensity plots and electric field spectrum analyzer data for Orbit 36 on November 26, 1971. The notations are the same as for Figure 7. In addition, between 1520 UT and 1600 UT a moderately strong half-gyrofrequency whistler-mode emission band is evident in the 16.5 kHz and 10.0 kHz electric field channels.

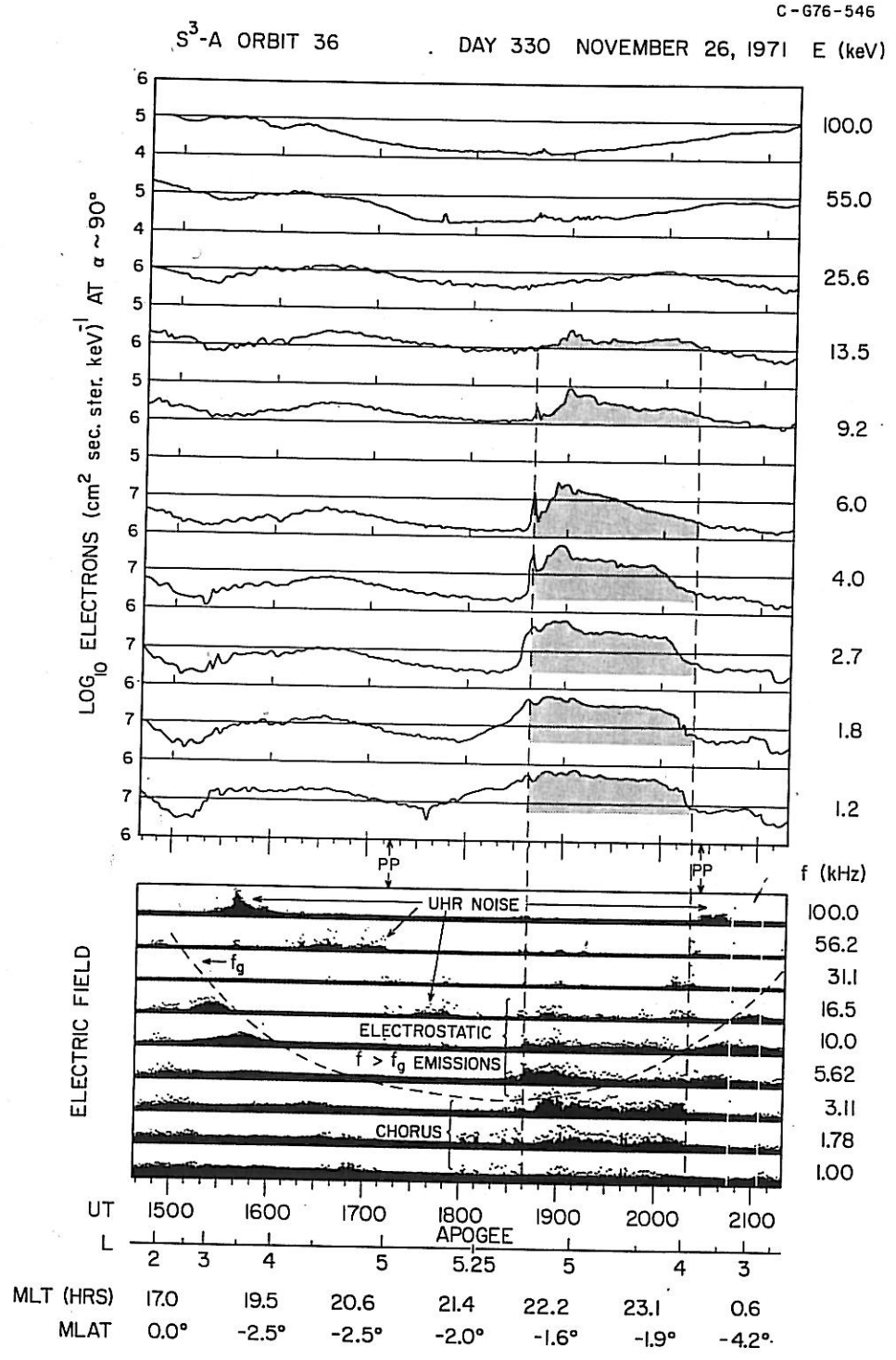
C-G76-546
S3-A ORBIT 36
DAY 330 NOVEMBER 26, 1971
E (keV)
100.0
55.0
25.6
13.5
9.2
6.0
4.0
2.7
1.8
1.2
LOG10 ELECTRONS (cm2 sec. ster. keV)-1 AT α ~ 90°
PP
PP
f (kHz)
100.0
56.2
31.1
16.5
10.0
5.62
3.11
1.78
1.00
UHR NOISE
fg
ELECTROSTATIC
f > fg EMISSIONS
CHORUS
ELECTRIC FIELD
UT 1500 1600 1700 1800 1900 2000 2100
APOGEE
L 2 3 4 5 5.25 5 4 3
MLT (HRS) 17.0 19.5 20.6 21.4 22.2 23.1 0.6
MLAT 0.0° -2.5° -2.5° -2.0° -1.6° -1.9° -4.2°

Figure 11

Figure 12 Electron intensity plots and electric field spectrum analyzer data for Orbit 115 on December 22, 1971. The top portion contains plots of the differential directional electron intensity, electrons $(cm^2 \text{ sec ster keV})^{-1}$, at $\alpha \sim 90°$ for electrons with mean energies from 1.8 keV to 400 keV for the time period 0500 UT to 1000 UT. The bottom portion displays the electric field digital spectrum analyzer output from 35 Hz to 100 kHz for the same time period. The measured electron gyrofrequency, f_g, has been drawn in as a dashed line. PP indicates the plasmapause locations. The shaded area on the low energy electron plots highlights the enhanced low energy electron intensities. For this orbit, the low energy electron enhancement and the moderately intense chorus bands begin and end nearly coincident with the outbound and inbound plasmapause crossings. The electrostatic $f > f_g$ emissions begin slightly before the low energy electron enhancement begins and end slightly after it ceases.

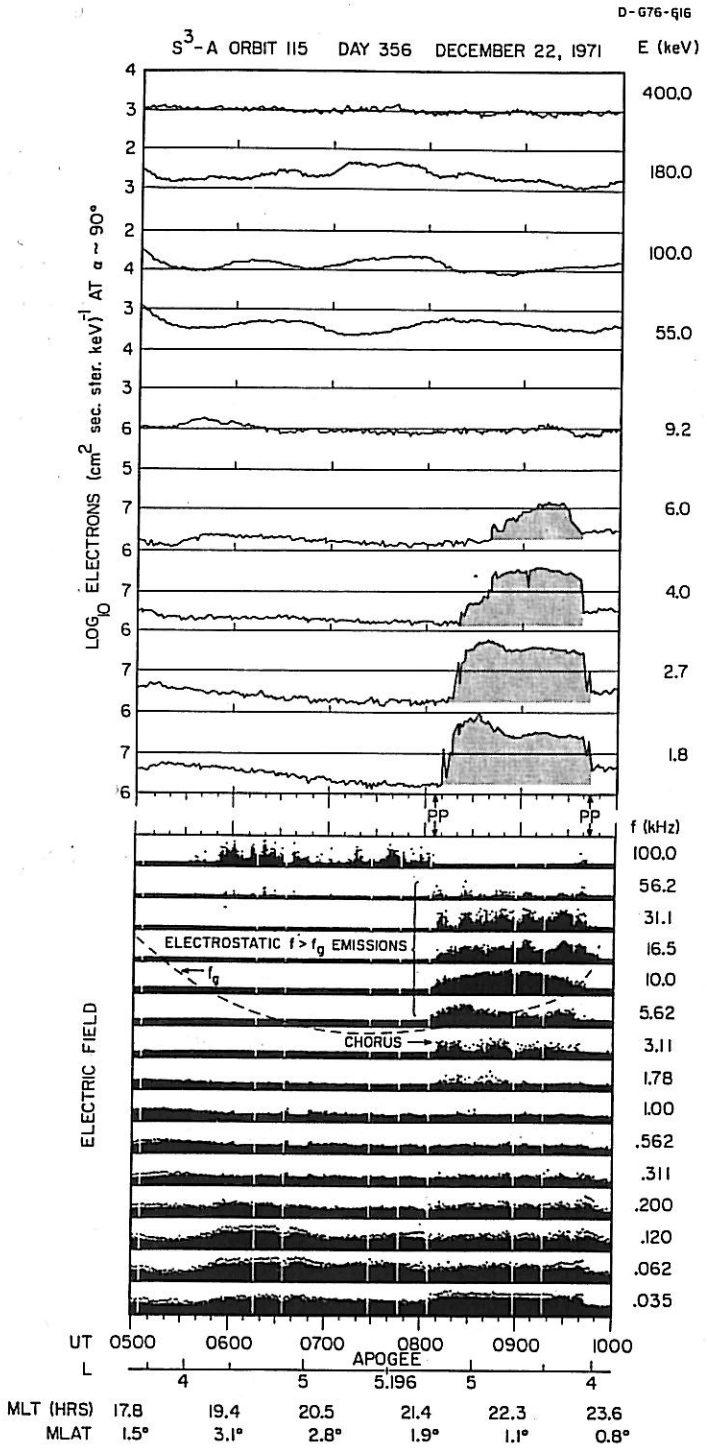
D-G76-616
S3-A ORBIT 115 DAY 356 DECEMBER 22, 1971
E (keV)
400.0
180.0
100.0
55.0
9.2
6.0
4.0
2.7
1.8
LOG10 ELECTRONS (cm2 sec. ster. keV)-1 AT α ~ 90°
PP
PP
f (kHz)
100.0
56.2
31.1
16.5
10.0
5.62
3.11
1.78
1.00
.562
.311
.200
.120
.062
.035
ELECTROSTATIC f > fg EMISSIONS
fg
CHORUS
ELECTRIC FIELD
UT 0500 0600 0700 0800 0900 1000
APOGEE
L 4 5 5.196 5 4
MLT (HRS) 17.8 19.4 20.5 21.4 22.3 23.6
MLAT 1.5° 3.1° 2.8° 1.9° 1.1° 0.8°

Figure 12

Figure 13 Electron intensity plots and wideband electric field data for Orbit 115. The top portion contains plots of the differential directional electron intensity at $\alpha \sim 90°$ for electrons with mean energies from 1.8 keV to 400 keV for the time period 0730 UT to 1000 UT. The bottom portion is a frequency-time spectrogram of the electric field wideband analog data for the same time period. The moderately intense chorus bands begin and end coincident with the low energy electron enhancement and nearly coincident with the out bound and inbound plasmapause crossings which are indicated by PP. The electrostatic $f > f_g$ emissions slightly precede both the outbound plasmapause crossing and the low energy electron enhancement.

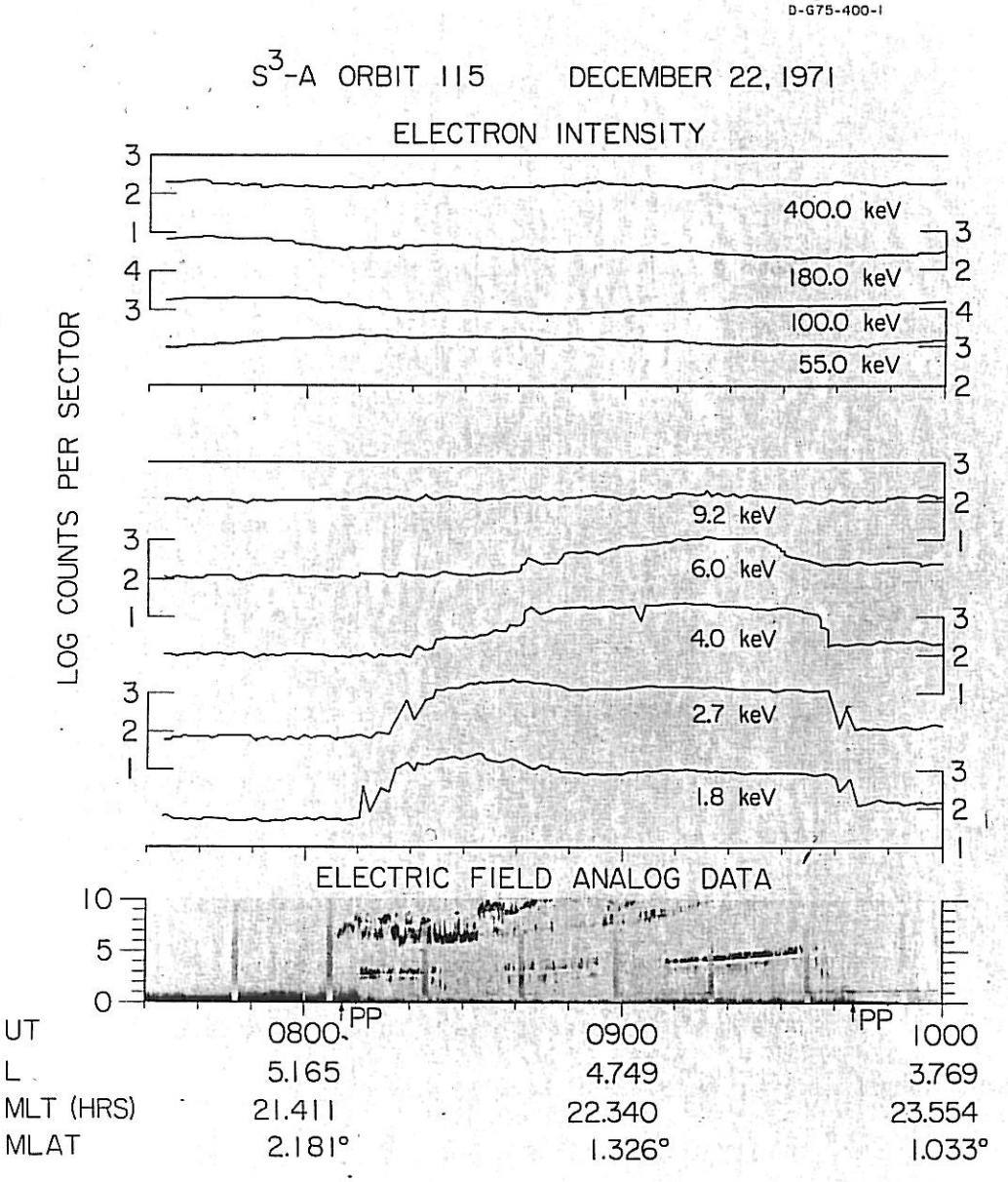
D-G75-400-1
S3-A ORBIT 115 DECEMBER 22, 1971
ELECTRON INTENSITY
LOG COUNTS PER SECTOR
400.0 keV
180.0 keV
100.0 keV
55.0 keV
9.2 keV
6.0 keV
4.0 keV
2.7 keV
1.8 keV
ELECTRIC FIELD ANALOG DATA
10
5
0
PP
PP
UT
0800
0900
1000
L
5.165
4.749
3.769
MLT (HRS)
21.411
22.340
23.554
MLAT
2.181°
1.326°
1.033°

Figure 13

Figure 14 Schematic diagram of equatorial cross-sections of the magnetosphere and the S^3-A orbit. The plasmasphere is indicated by light shading bounded by a dashed line. The dusk to dawn plasma sheet is indicated by the dark shading. Panel (a) shows a typical November-December S^3-A orbit. The plasmasphere boundary shown is for the average plasmasphere during moderately disturbed periods following Carpenter [1966]. For moderately disturbed periods an electron trough, a region nearly void of electrons, with a width of 1-3 earth radii usually separates the plasmasphere and the plasma sheet in the evening sector prior to midnight. Panels (b), (c), and (d) show the magnetosphere for Orbits 35, 36 and 115, respectively. The plasmasphere and plasma sheet for each orbit have been modified to agree with the satellite measurements of the plasmapause locations and the low energy electron enhancements. The hatched lines show where the chorus and electrostatic $f > f_g$ emissions are observed. For Orbits 35 and 36 the satellite passes through the electron trough before the low energy electrons are encountered and the emissions are observed.

Figure 14 (cont'd.) For Orbit 115 the electron trough has been filled in several hours prior to midnight and the satellite passes directly from the plasmasphere to the plasma sheet.

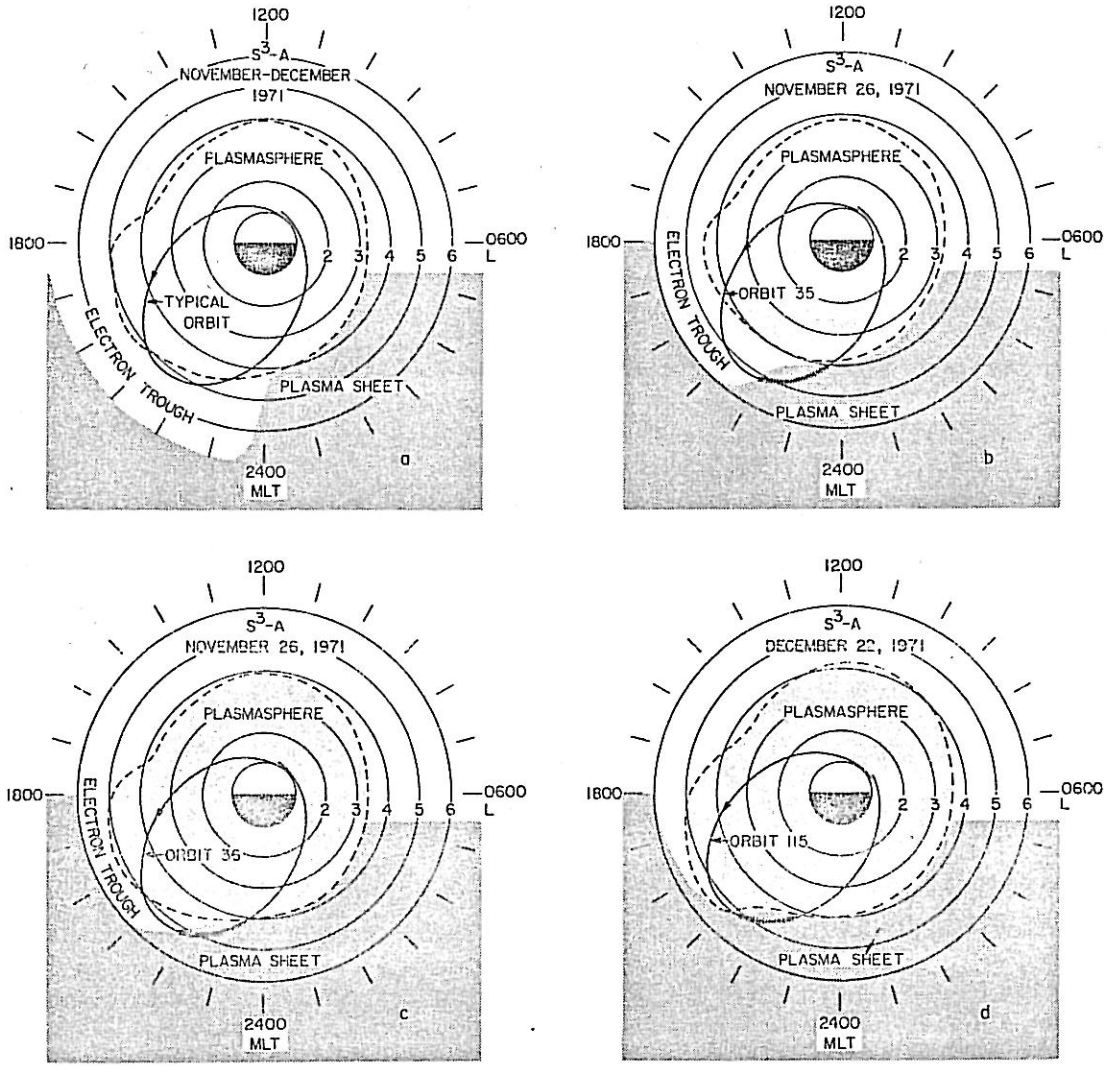
1200
S3-A
NOVEMBER-DECEMBER
1971
PLASMASPHERE
1800
0600
L
2
3
4
5
6
TYPICAL
ORBIT
ELECTRON TROUGH
PLASMA SHEET
2400
MLT
a
1200
S3-A
NOVEMBER 26, 1971
PLASMASPHERE
1800
0600
L
ELECTRON TROUGH
ORBIT 35
PLASMA SHEET
2400
MLT
b
1200
S3-A
NOVEMBER 26, 1971
PLASMASPHERE
1800
0600
L
ELECTRON TROUGH
ORBIT 35
PLASMA SHEET
2400
MLT
c
1200
S3-A
DECEMBER 22, 1971
PLASMASPHERE
1800
0600
L
ORBIT 115
PLASMA SHEET
2400
MLT
d

Figure 14

Figure 15 Comparison between whistler-mode spectra and electron pitch angle distributions. At the top are the wideband analog frequency-time spectrograms for the magnetic and electric field data for 1833 UT to 1927 UT for Orbit 36. For this illustration time increases from right to left. The bottom contains plots of the pitch angle distributions at five minute intervals for electrons from 1.2 keV to 25.6 keV. For each small square the scale on the axis of abscissas is 0° to 180° pitch angle and the scale on the axis of ordinates is $\log_{10}$ electrons $(cm^2$ sec ster keV$)^{-1}$ and full scale covers five orders of magnitude of electron intensity. The slanted lines between the bottom of the electric field spectrogram and the top of the pitch angle plots show when the pitch angle plots were made. Note that the intense chorus band from 1848 UT to 1903 UT with frequencies almost entirely greater than 0.5 f_g occurs simultaneously with extremely anisotropic pitch angle distributions, especially for the 4.0 and 6.0 keV electrons.

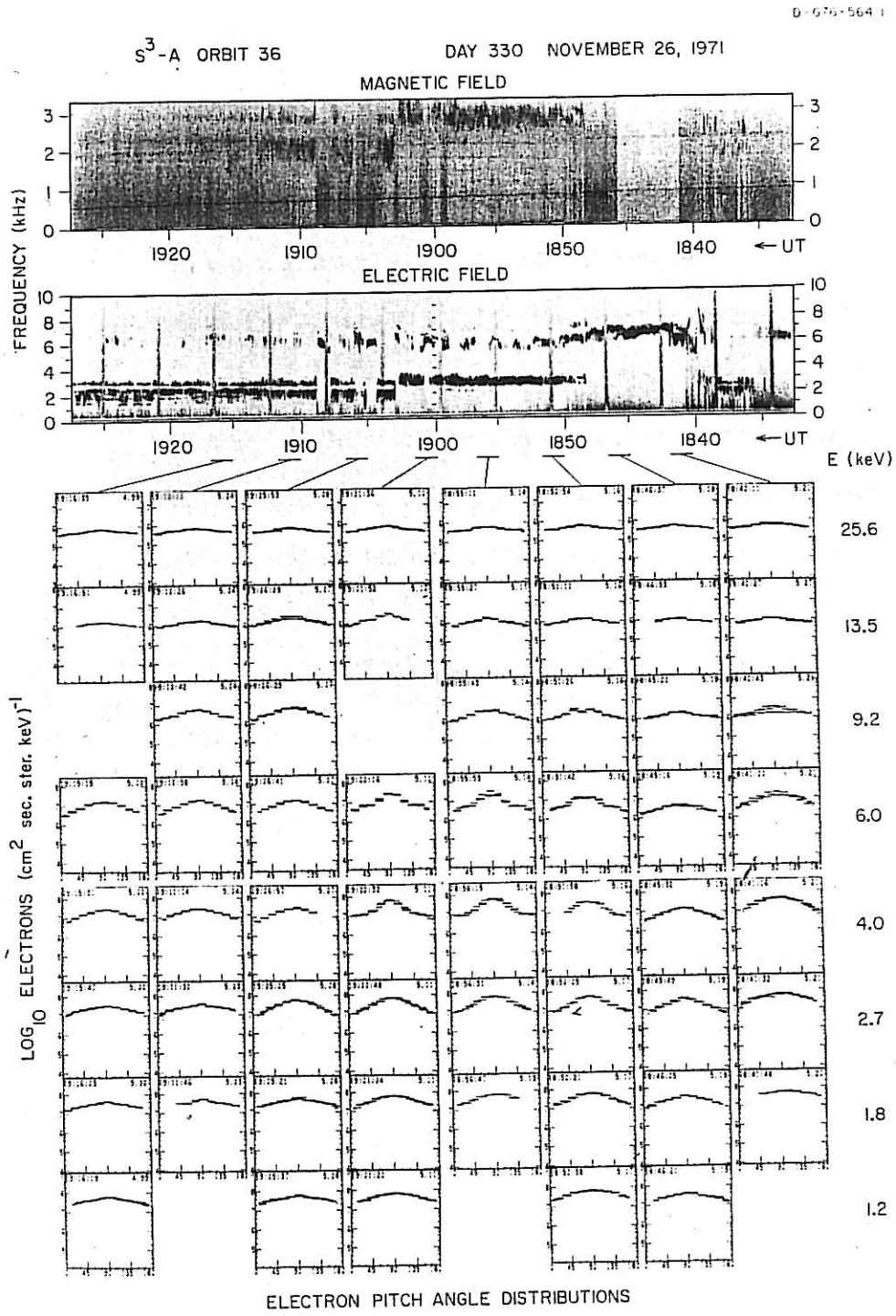
D-676-564-1
S3-A ORBIT 36
DAY 330 NOVEMBER 26, 1971
MAGNETIC FIELD
FREQUENCY (kHz)
3
2
1
0
1920
1910
1900
1850
1840
←UT
ELECTRIC FIELD
10
8
6
4
2
0
E (keV)
25.6
13.5
9.2
6.0
4.0
2.7
1.8
1.2
LOG10 ELECTRONS (cm2 sec. ster. keV)-1
ELECTRON PITCH ANGLE DISTRIBUTIONS

Figure 15

Figure 16 Comparison between chorus spectra and electron pitch angle distributions around 1903 UT for Orbit 36. The top contains an electric field frequency-time spectrogram from 1853 UT to 1914 UT. The bottom contains the electron pitch angle distributions at ~ 1902:30 and 1904:40 for 4.0 and 6.0 keV. Note that the rapid change from a very anisotropic to a less anisotropic pitch angle distribution exactly coincides with the chorus spectra changing from having frequency components almost only above $f_g/2$ to having lower frequency components both above and below $f_g/2$.

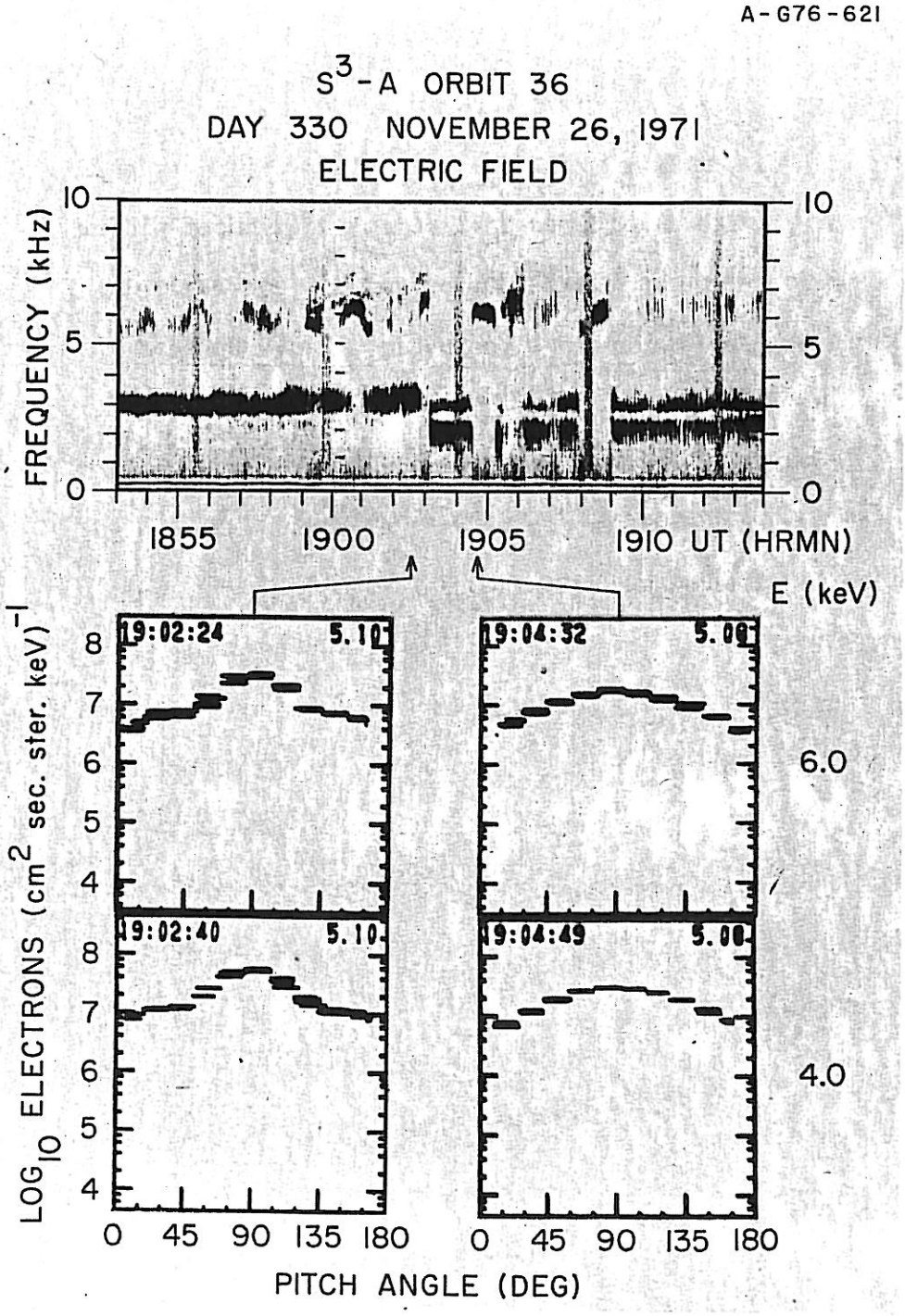
A-G76-621
S3-A ORBIT 36
DAY 330 NOVEMBER 26, 1971
ELECTRIC FIELD
FREQUENCY (kHz)
10
5
0
1855
1900
1905
1910 UT (HRMN)
E (keV)
LOG10 ELECTRONS (cm2 sec. ster. keV)-1
19:02:24
19:02:40
19:04:32
19:04:49
6.0
4.0
0 45 90 135 180
PITCH ANGLE (DEG)

Figure 16

Figure 17 Electron pitch angle distributions for Orbit 115 at one minute intervals from 0831 UT to 0833 UT and 0858 UT to 0900 UT for 1.8 keV to 400 keV. Near 0832 UT the 2.7 keV and 4.0 keV pitch angle distributions are nearly flat from $\alpha \sim 55°$ to $\alpha \sim 125°$ or even display a relative minimum near $\alpha \sim 90°$. Around 0900 UT the 6.0 keV pitch angle distribution is flat if not slightly concave from $\alpha \sim 60°$ to $\alpha \sim 120°$. These flat or concave distributions occur simultaneously with significantly decreased chorus amplitudes as can be seen from ~ 0826 UT to ~ 0837 UT and from ~ 0856 UT to ~ 0908 UT in Figures 12 and 13. The flat or concave distributions occur at energies appropriate for cyclotron resonance with the chorus and thus can cause damping.

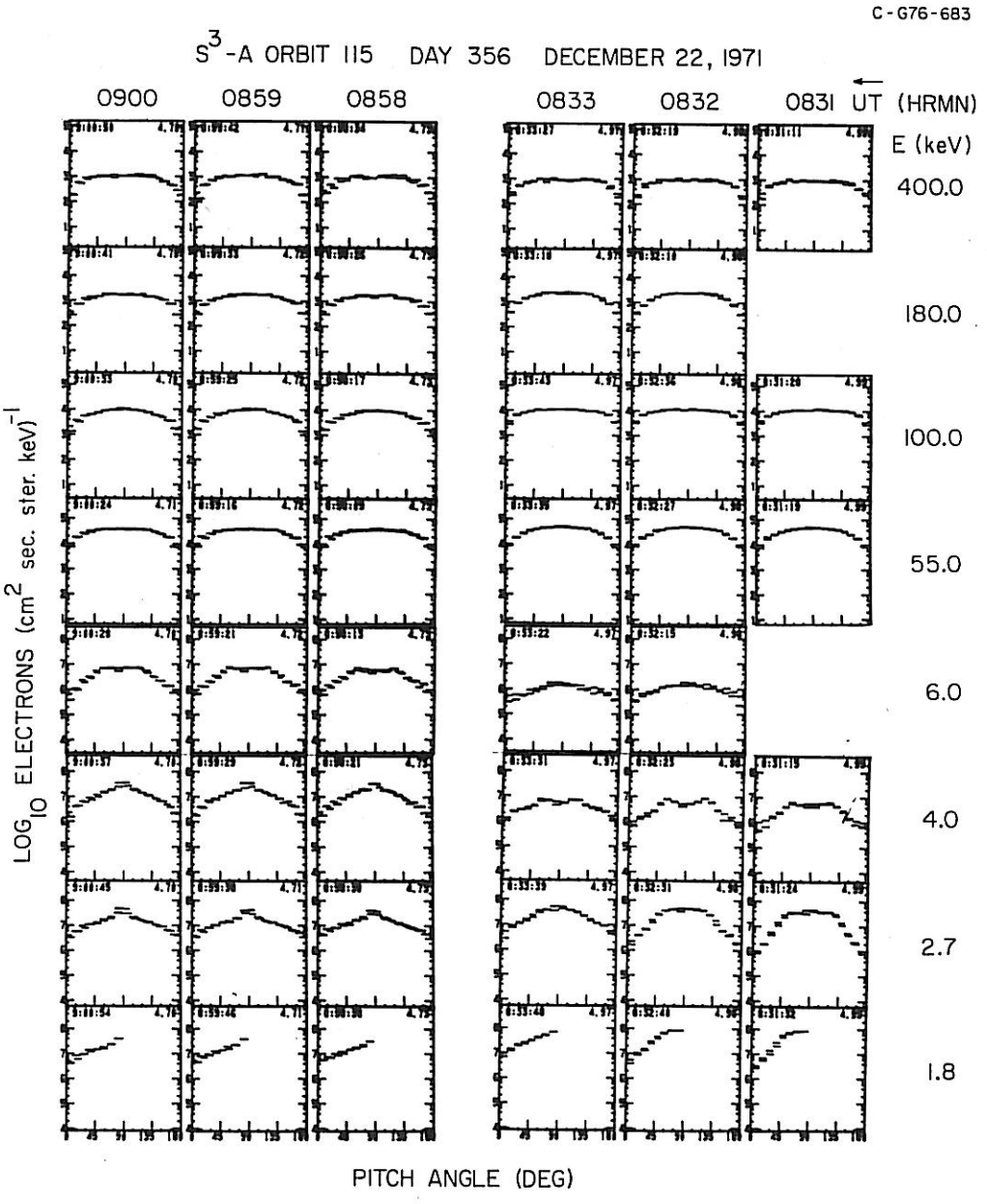
C-G76-683
S3-A ORBIT 115 DAY 356 DECEMBER 22, 1971
0900
0859
0858
0833
0832
0831 UT (HRMN)
E (keV)
400.0
180.0
100.0
55.0
6.0
4.0
2.7
1.8
LOG10 ELECTRONS (cm2 sec. ster. keV)-1
PITCH ANGLE (DEG)

Figure 17

Figure 18 Pitch angle distributions for 1.2 keV to 25.6 keV electrons for Orbit 36 from 1535 UT to 1610 UT. The rather anisotropic distribution prior to 1600 UT occurs simultaneously with half-gyrofrequency whistler-mode waves evident in Figure 11. Following 1600 UT the pitch angle distributions become nearly isotropic and little evidence of the half-gyrofrequency whistler-mode waves appear after 1600 UT. Note that although the pitch angle distributions become less anisotropic, the $\alpha \sim 90°$ intensities remain nearly the same.

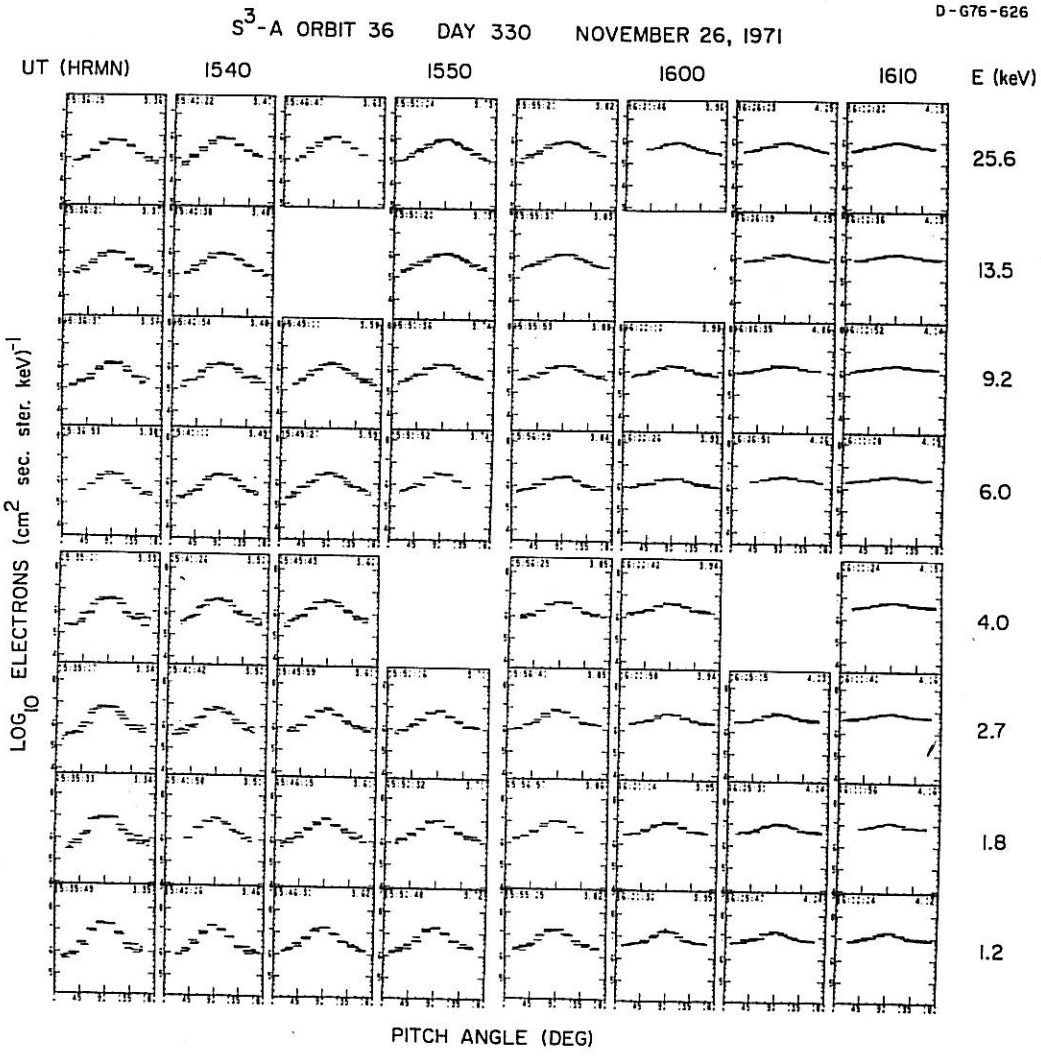
D-G76-626
S3-A ORBIT 36 DAY 330 NOVEMBER 26, 1971
UT (HRMN)
1540
1550
1600
1610
E (keV)
25.6
13.5
9.2
6.0
4.0
2.7
1.8
1.2
LOG10 ELECTRONS (cm2 sec. ster. keV)-1
PITCH ANGLE (DEG)

Figure 18

Figure 19 Differential directional electron intensities at $\alpha \sim 90°$ from 1.2 keV to 100 keV and electric field digital spectrum analyzer output from 35 Hz to 100 kHz for Orbit 67 on December 6, 1971. PP indicates the plasmapause crossings. As indicated by the shaded area, only the lowest energy electrons are enhanced. Correspondingly in the electric field data only electrostatic $f > f_g$ emissions are present outside the plasmasphere. No chorus emissions are evident.

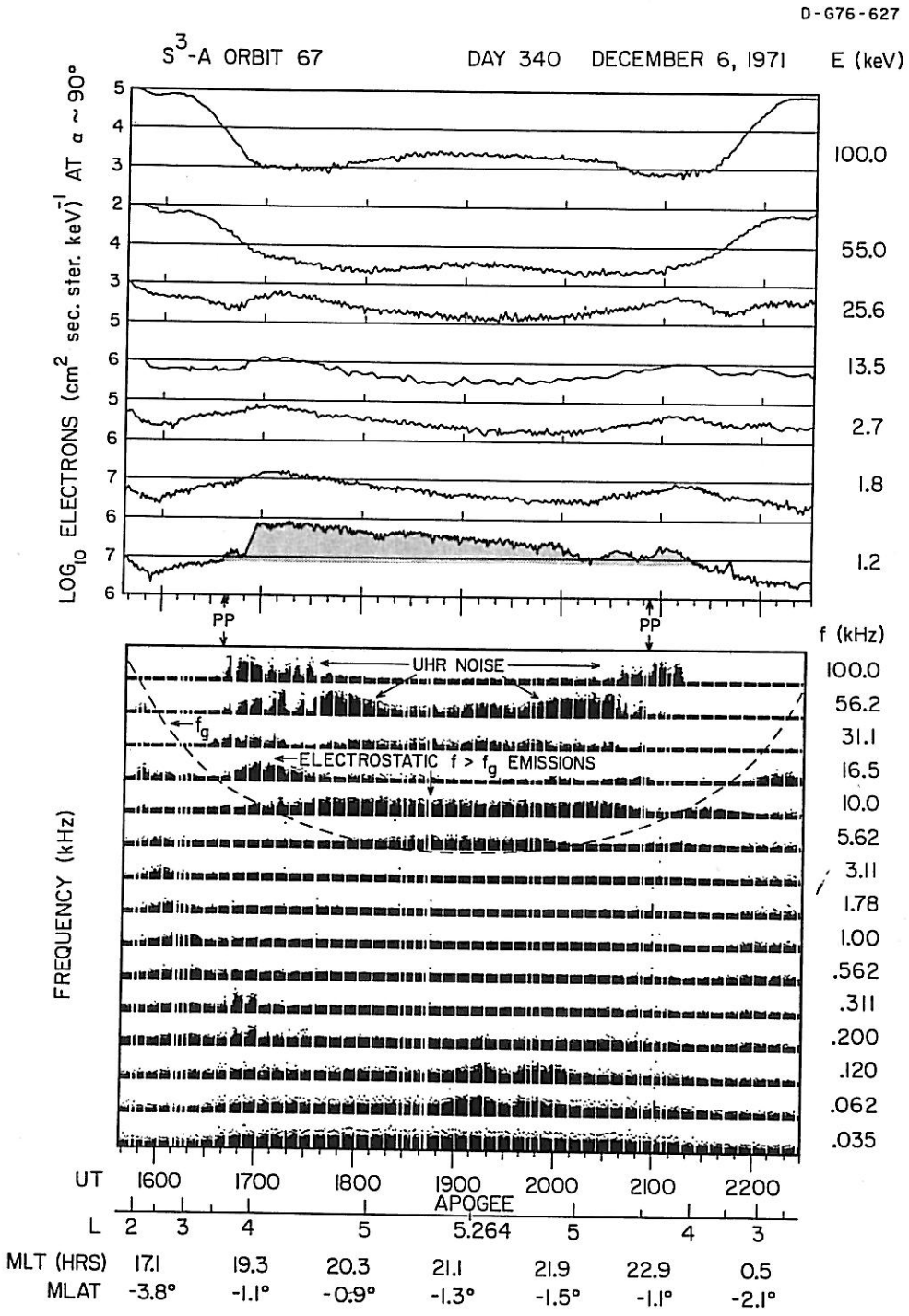
D-G76-627
S3-A ORBIT 67
DAY 340 DECEMBER 6, 1971
E (keV)
LOG10 ELECTRONS (cm2 sec. ster. keV)-1 AT α ~ 90°
100.0
55.0
25.6
13.5
2.7
1.8
1.2
PP
PP
f (kHz)
UHR NOISE
fg
ELECTROSTATIC f > fg EMISSIONS
FREQUENCY (kHz)
100.0
56.2
31.1
16.5
10.0
5.62
3.11
1.78
1.00
.562
.311
.200
.120
.062
.035
UT 1600 1700 1800 1900 2000 2100 2200
APOGEE
L 2 3 4 5 5.264 5 4 3
MLT (HRS) 17.1 19.3 20.3 21.1 21.9 22.9 0.5
MLAT -3.8° -1.1° -0.9° -1.3° -1.5° -1.1° -2.1°

Figure 19

Figure 20 Electric field wideband analog data from 1800 UT to 2100 UT for Orbit 67. Only electrostatic $f > f_g$ emissions are present. Note that the frequency of the emission bands changes quasiperiodically from being above 1.5 f_g to being below 1.5 f_g. From 1830 UT to 1845 UT this change is nearly periodic with a period of ~ 67 seconds. Around 1940 UT the period is about 85 seconds. Throughout this time period shown in this figure, PC3 micropulsations were observed by the ground station at College, Alaska. From ~ 1850 UT to ~ 1905 UT the micropulsations were quite periodic with a period of ~ 63 seconds.

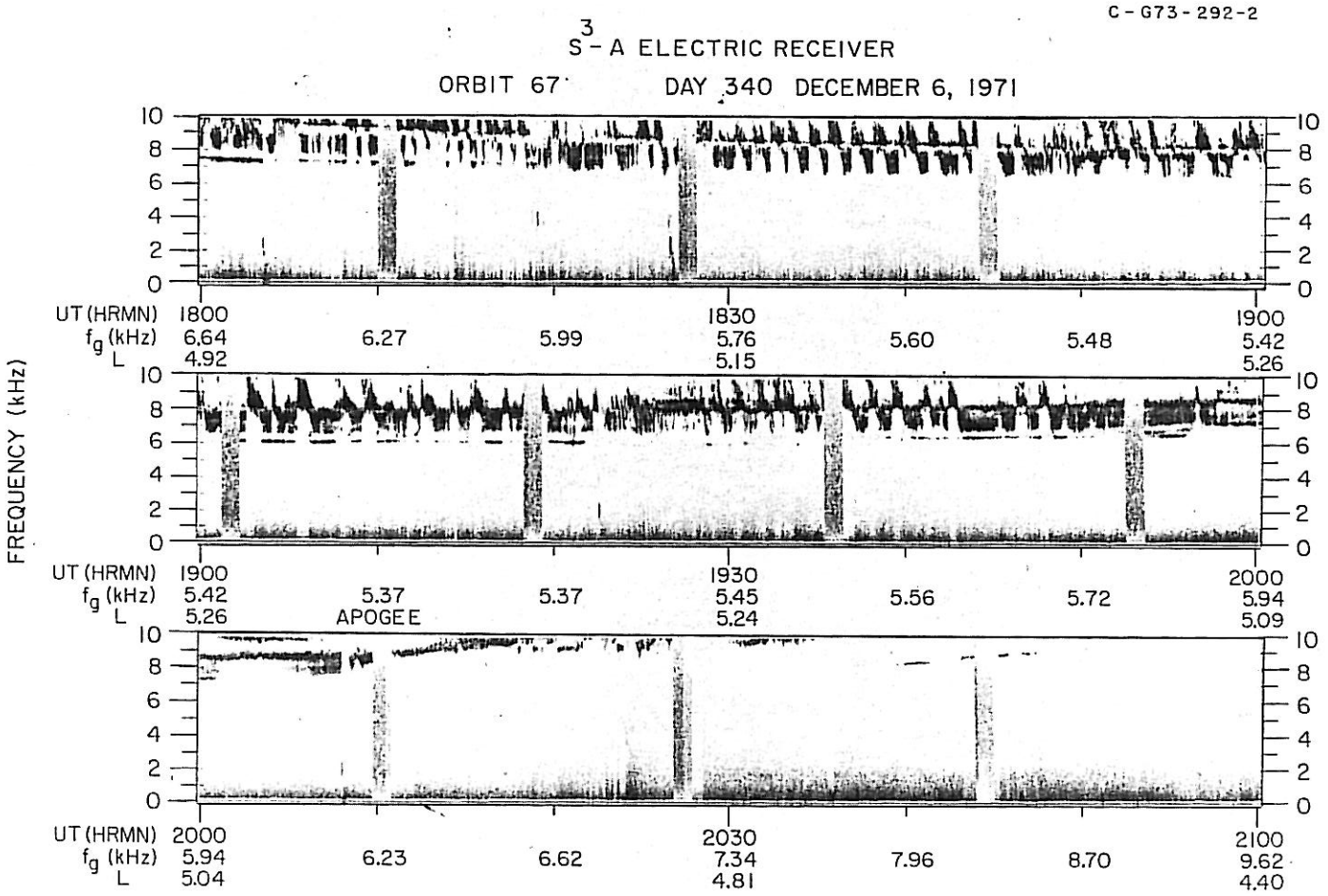
C-G73-292-2
S3-A ELECTRIC RECEIVER
ORBIT 67 DAY 340 DECEMBER 6, 1971
FREQUENCY (kHz)
UT (HRMN) 1800 1830 1900
fg (kHz) 6.64 6.27 5.99 5.76 5.60 5.48 5.42
L 4.92 5.15 5.26
UT (HRMN) 1900 1930 2000
fg (kHz) 5.42 5.37 5.37 5.45 5.56 5.72 5.94
L 5.26 APOGEE 5.24 5.09
UT (HRMN) 2000 2030 2100
fg (kHz) 5.94 6.23 6.62 7.34 7.96 8.70 9.62
L 5.04 4.81 4.40

Figure 20

Figure 21 $\alpha \sim 90°$ electron energy spectra at L = 5.2 for Orbits 66, 67 and 68 on December 6, 1971. Orbit 66 is plotted as closed triangles, Orbit 67 is plotted as closed circles and Orbit 68 is plotted as x's. We have also plotted the mean quiet time spectra at L = 5.2 for Orbits 75-97. As indicated by the shaded area, only the lowest energy electrons for Orbit 67 are enhanced.

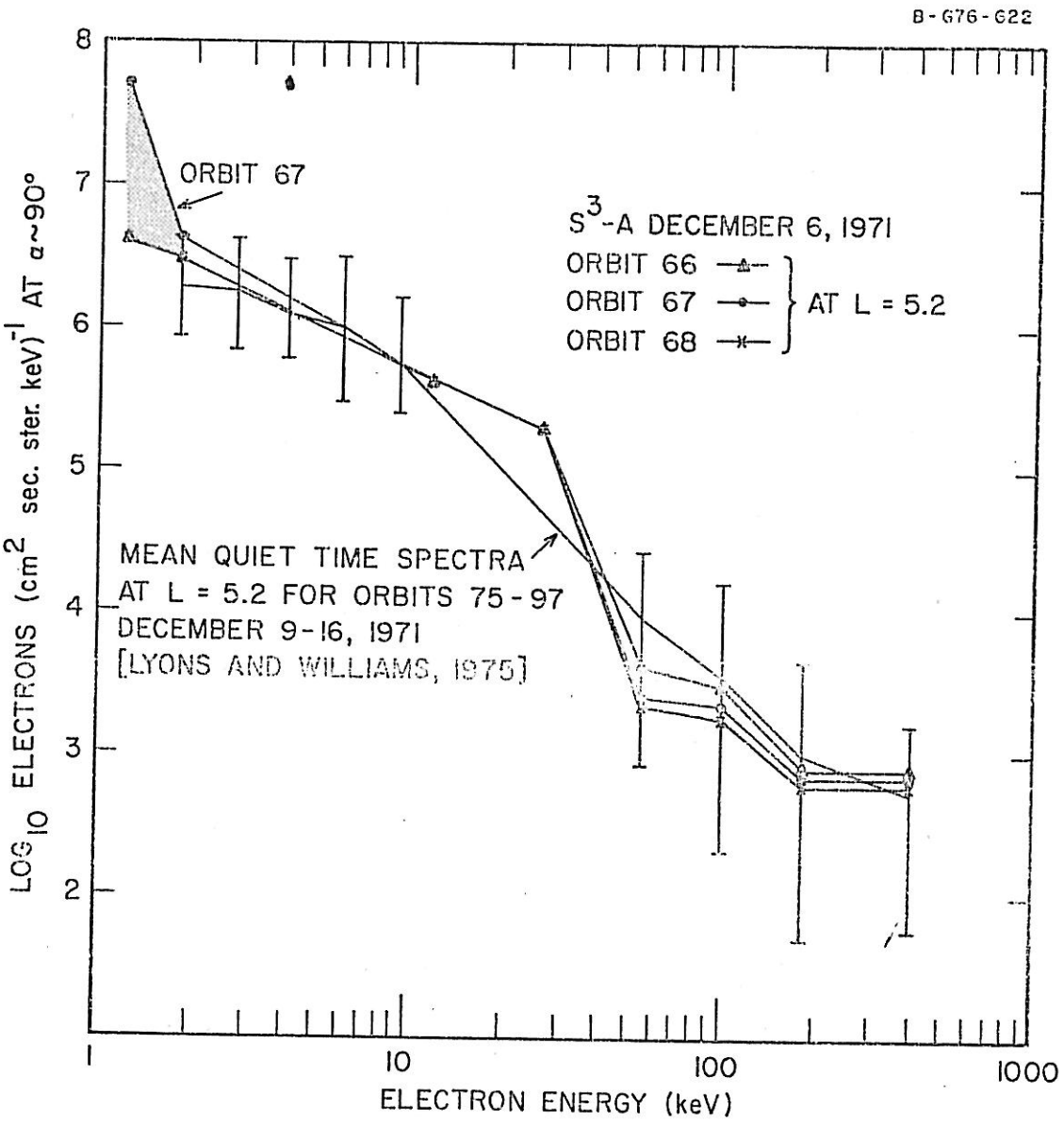
B-676-622
ORBIT 67
S3-A DECEMBER 6, 1971
ORBIT 66
ORBIT 67
ORBIT 68
AT L = 5.2
MEAN QUIET TIME SPECTRA
AT L = 5.2 FOR ORBITS 75-97
DECEMBER 9-16, 1971
[LYONS AND WILLIAMS, 1975]
LOG10 ELECTRONS (cm2 sec. ster. keV)-1 AT α~90°
ELECTRON ENERGY (keV)
8
7
6
5
4
3
2
1
10
100
1000

Figure 21

Figure 22 Pitch angle distributions from 1730 UT to 1745 UT on Orbit 67 for electrons from 1.2 keV to 400 keV. The 1.2 keV pitch angle distributions are extremely anisotropic, the 1.8 keV distributions are mildly anisotropic and all higher energy distributions are nearly isotropic.

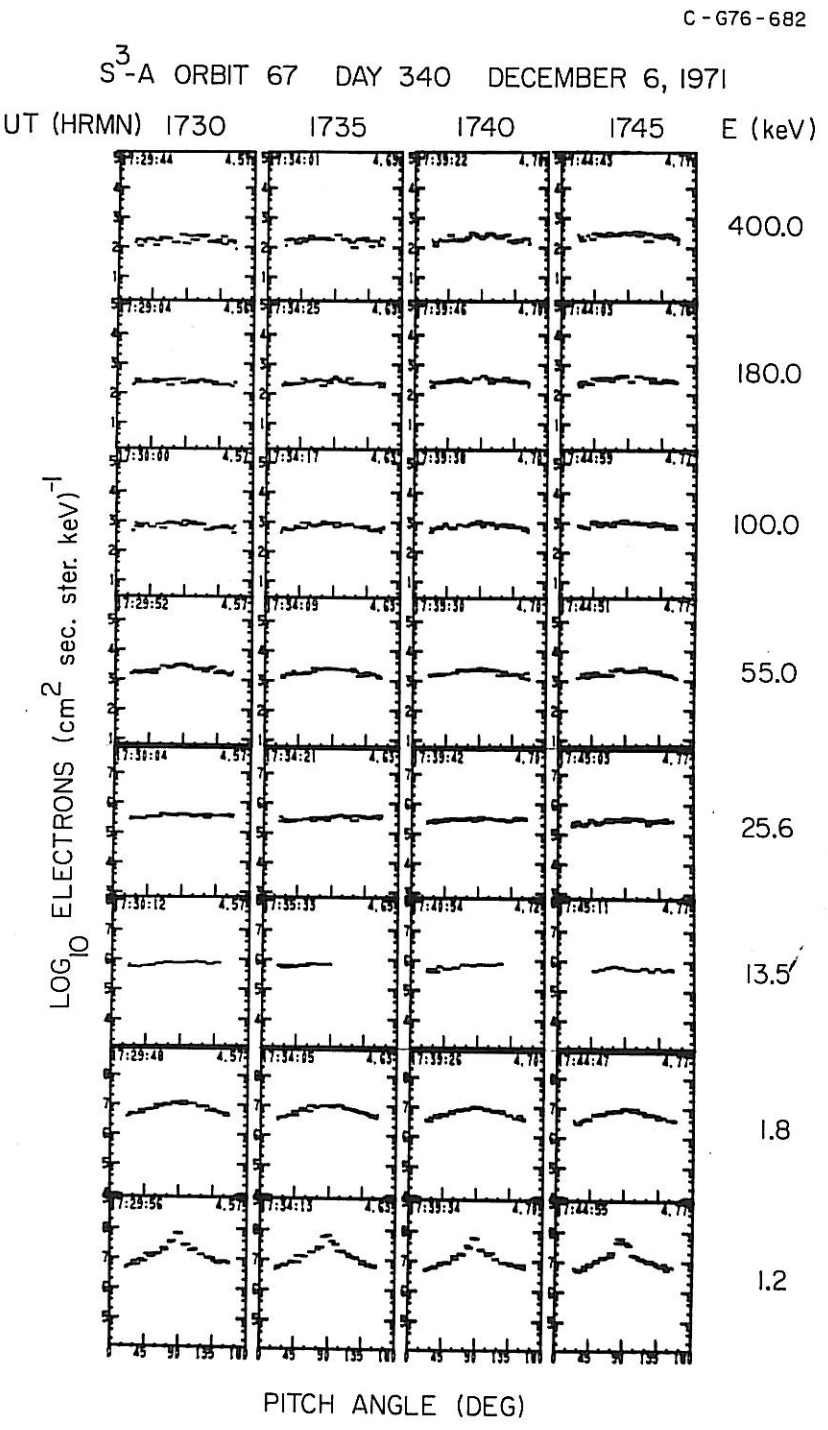
C-G76-682
S3-A ORBIT 67 DAY 340 DECEMBER 6, 1971
UT (HRMN) 1730
1735
1740
1745
E (keV)
400.0
180.0
100.0
55.0
25.6
13.5
1.8
1.2
LOG10 ELECTRONS (cm2 sec. ster. keV)-1
PITCH ANGLE (DEG)

Figure 22

Figure 23 Calculated growth rate plots for L = 5.2 and L = 4.9 on Orbit 35. N = 10 cm^{-3} was used for both calculations but f_g was adjusted according to the measured magnetic field. At L = 5.2, as shown in panel (a), which was prior to the anisotropic electron enhancement only weak growth up to ~ 0.3 f_g could be supported by the observed electron distributions. At L = 4.9, as shown in panel (b), which was during the anisotropic electron enhancement, strong wave growth from ~ 0.29 f_g and up to ~ 0.55 f_g could be supported by the observed enhanced electron distributions. In panel (b) in addition to the growth rate for the m = -1 cyclotron resonance for parallel propagation ($\theta = 0°$), we have also plotted the growth rates for the m = -1 resonance at wave normal angles $\theta = 10°$, 20° and 30° and the m = 0 (Landau resonance) damping rate for $\theta = 10°$.

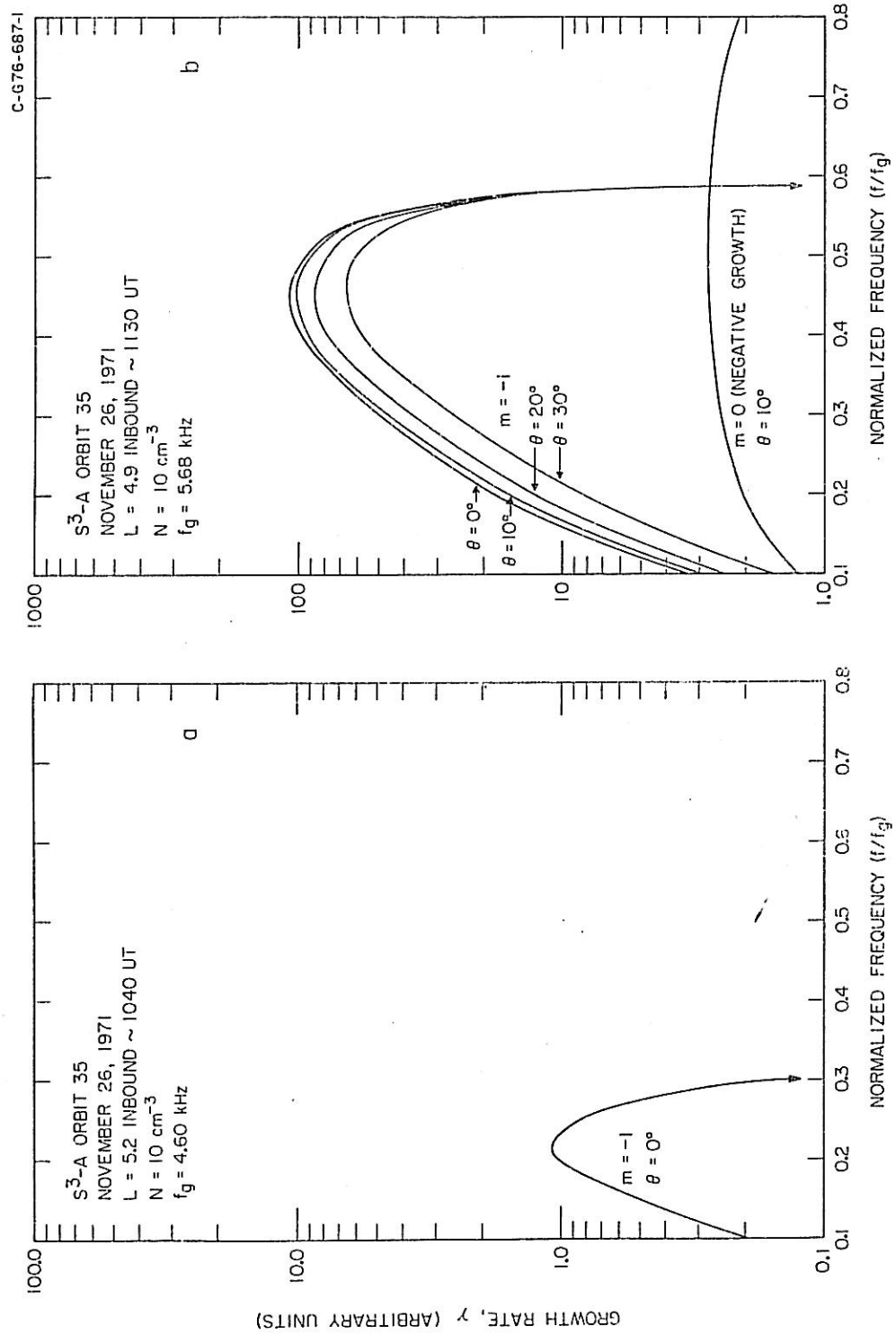
C-G76-687-1
S3-A ORBIT 35
NOVEMBER 26, 1971
L = 5.2 INBOUND ~ 1040 UT
N = 10 cm-3
fg = 4.60 kHz
a
m = -1
θ = 0°
S3-A ORBIT 35
NOVEMBER 26, 1971
L = 4.9 INBOUND ~ 1130 UT
N = 10 cm-3
fg = 5.68 kHz
b
θ = 0°
θ = 10°
m = -1
θ = 20°
θ = 30°
m = 0 (NEGATIVE GROWTH)
θ = 10°
GROWTH RATE, γ (ARBITRARY UNITS)
NORMALIZED FREQUENCY (f/fg)
NORMALIZED FREQUENCY (f/fg)

Figure 23

Figure 24 Calculated growth rate plot for ~ 1856 UT on Orbit 36 during a very anisotropic electron enhancement. For this calculation we used N = 8 cm^{-3} and f_g = 4.96 kHz. The calculation shows that the observed very anisotropic electron distribution would produce weak growth up to ~ 0.3 f_g and then negative growth (damping) up to 0.51 f_g. Strong growth is then produced up to 0.6 f_g. This pattern of growth is similar to the observed chorus spectra.

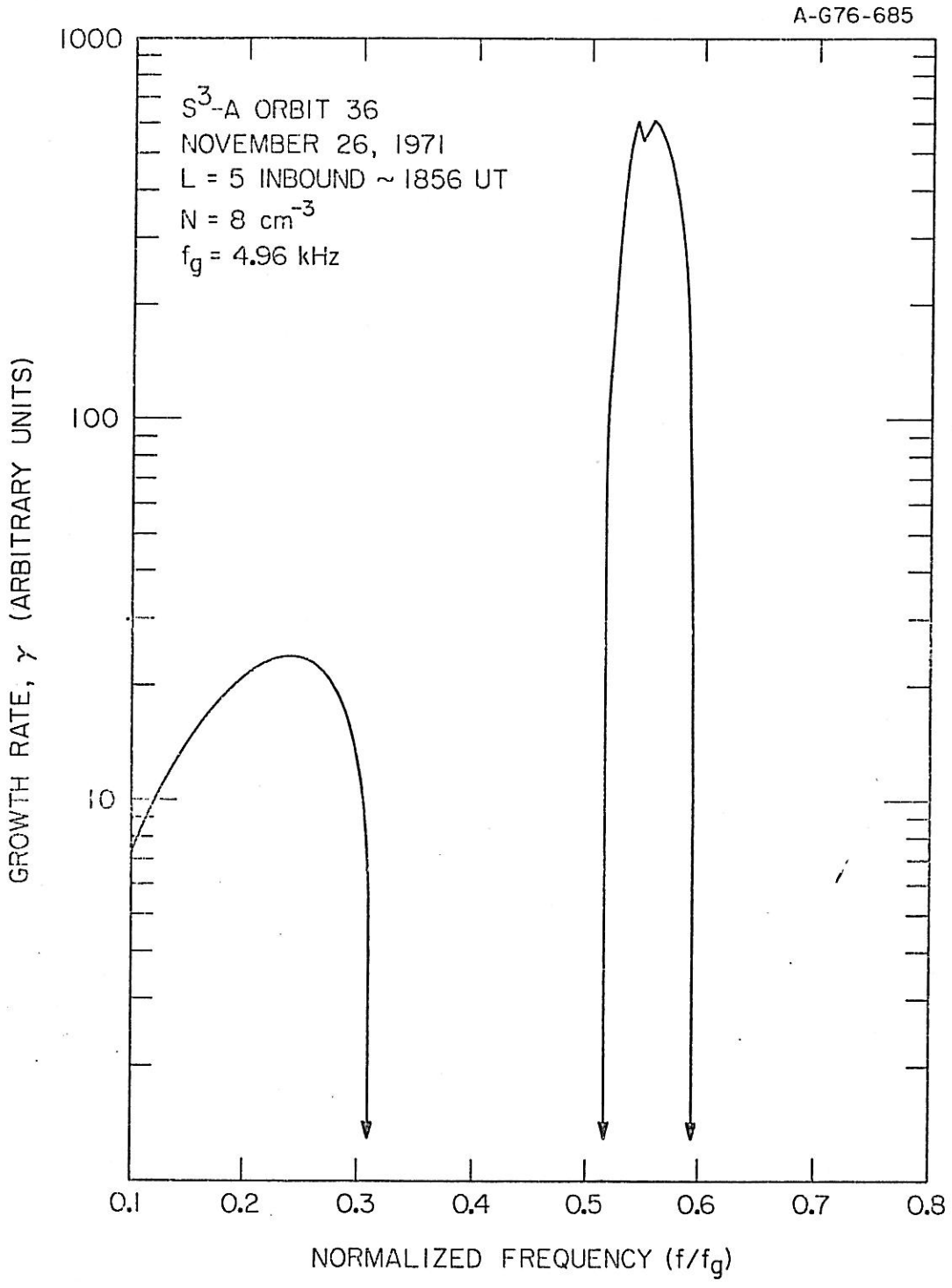
A-G76-685
1000
100
10
S^3-A ORBIT 36
NOVEMBER 26, 1971
L = 5 INBOUND ~ 1856 UT
N = 8 cm^{-3}
f_g = 4.96 kHz
GROWTH RATE, γ (ARBITRARY UNITS)
0.1
0.2
0.3
0.4
0.5
0.6
0.7
0.8
NORMALIZED FREQUENCY (f/f_g)

Figure 24

Figure 25 Calculated growth rate plot for the half-gyrofrequency whistler-mode noise observed prior to 1600 UT on Orbit 35. $N = 100\ cm^{-3}$ and $f_g = 19.9$ kHz. Strong growth is predicted from $0.25\ f_g$ up to $0.63\ f_g$.

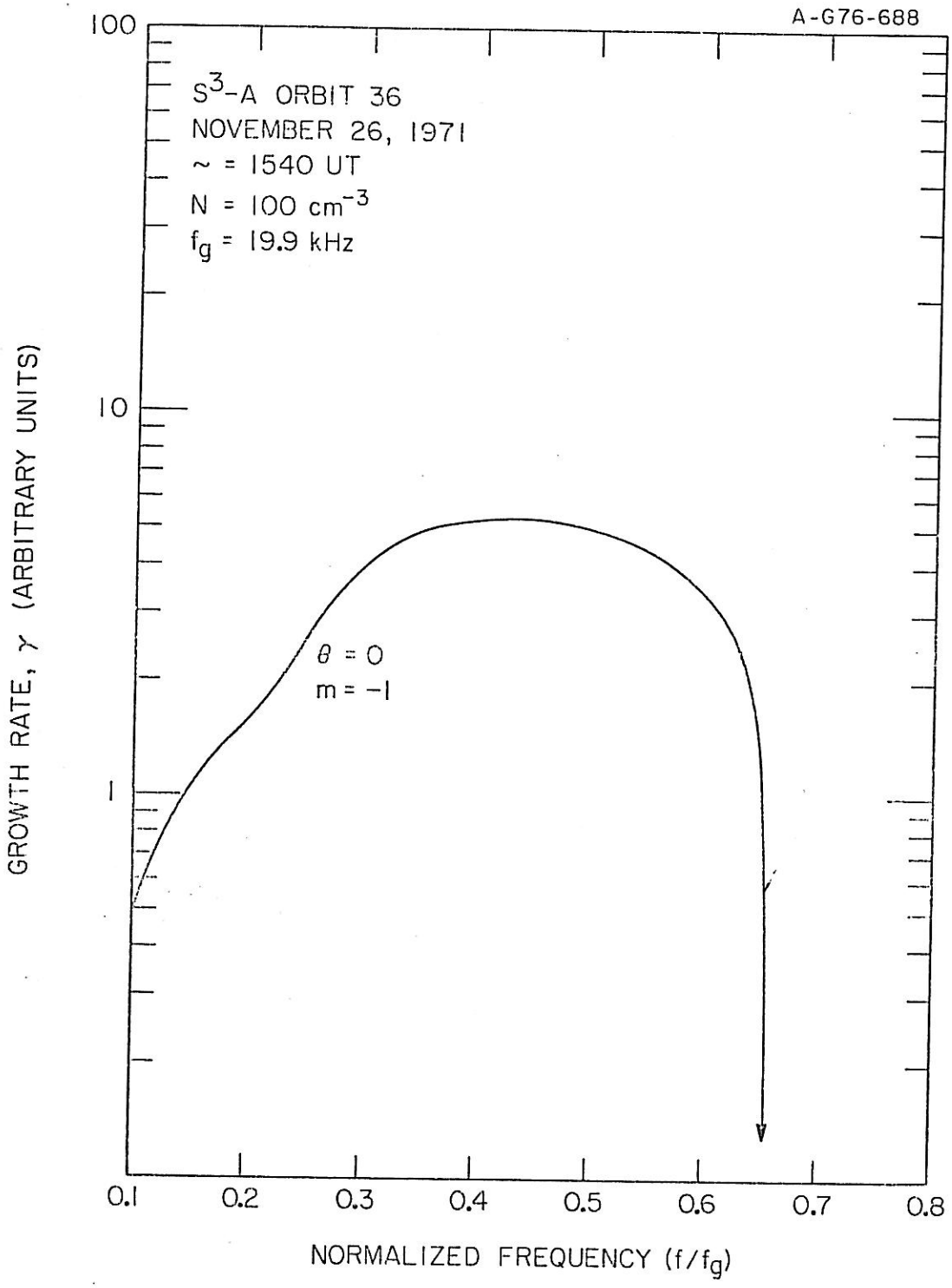
A-G76-688
S3-A ORBIT 36
NOVEMBER 26, 1971
~ = 1540 UT
N = 100 cm-3
fg = 19.9 kHz
θ = 0
m = -1
100
10
1
0.1
0.2
0.3
0.4
0.5
0.6
0.7
0.8
GROWTH RATE, γ (ARBITRARY UNITS)
NORMALIZED FREQUENCY (f/fg)

Figure 25